Nanoscale

REVIEW

View Article Online
View Journal | View Issue

Cite this: *Nanoscale*, 2022, **14**, 2966

Advanced composite glasses with metallic, perovskite, and two-dimensional nanocrystals for optoelectronic and photonic applications

I. Konidakis, * A. Karagiannaki and E. Stratakis *

This article reviews the tremendous advancement of the optoelectronic and photonic properties of inorganic oxide glasses upon the incorporation of metallic, perovskite, and two-dimensional nanocrystals within their matrix. In the first part, we present the exploitation of typical inorganic oxide glasses as hosting platforms for the incorporation of metallic nanoparticles. Such a method offers tremendous advantages in terms of inducing plasmonic features that enable the tunability of the photonic properties of the embedded materials. Along similar lines, due to their exceptional photoluminescence properties all inorganic lead halide perovskites show enormous potential for next generation light-emitting, optoelectronic and photonic devices. To date, however, their usage is limited significantly by their poor chemical stability upon exposure to moisture, and lead toxicity issues. A recent and highly promising approach for overcoming these important challenges is the encapsulation of perovskite nanocrystals within inorganic oxide glasses. Based on this, in the second section we focus on the recent advancements in perovskite glasses in terms of the developed fabrication procedures and the resulting optoelectronic features, while considering the production limitations. In the last part, we consider the development of composite two-dimensional materials glass architectures in terms of the available synthesis routes and the novelty of their optical and emission features. Finally, future perspectives on the described composite glass systems in terms of potential applications are summarized.

Received 22nd November 2021,
Accepted 17th January 2022

DOI: 10.1039/d1nr07711b

rsc.li/nanoscale

1. Introduction

Inorganic oxide glasses are impressive materials that have been used in a variety of applications for almost a century. There are three main definitions of what type of material can

Institute of Electronic Structure and Laser (IESL), Foundation for Research and Technology-Hellas (FORTH), 70013 Heraklion-Crete, Greece.
E-mail: ikonid@iesl.forth.gr, stratak@iesl.forth.gr

I. Konidakis

Dr Ioannis Konidakis was born in Crete, Greece, in 1980. He has a B.Sc. Honours degree in Chemistry from the University of Aberdeen in the UK (2002). He received his Ph.D. degree in Chemistry from the same University in 2006. In his present IESL research appointment he is part of the Ultrafast Laser Micro- and Nano-Processing (ULMNP) Laboratory. His research interests are focused on the synthesis and characterization of composite glasses and energy harvesting materials for advanced photonic, thermoelectric, and photovoltaic applications.

A. Karagiannaki

Anna Karagiannaki is an MSc student at the Department of Chemistry at the University of Crete, Greece. She received her BSc degree in Chemistry from the same department in 2019. She joined the Ultrafast Laser Micro- and Nano-Processing Group of IESL-FORTH during the undergraduate program and studied the micro-nano structuring of semiconducting materials as well as their wettability properties. Her current research interests include the synthesis and characterization of composite glasses.

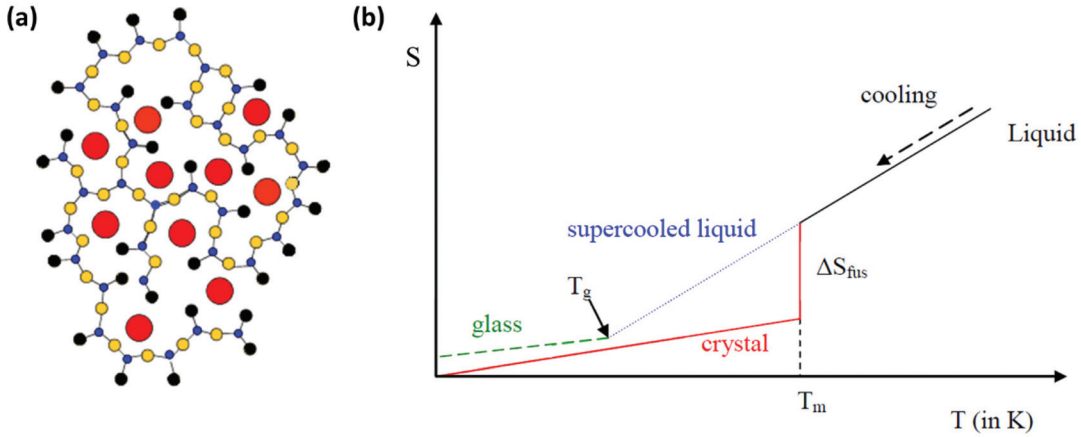

Fig. 1 (a) Schematic representation of the sodium silicate glass network in two dimensions. Red circles represent sodium cations, blue circles represent silicon atoms, yellow circles represent bridging oxygen atoms, and black circles represent non-bridging oxygen atoms (a has been adapted from ref. 4 with permission from John Wiley and Sons, copyright 2006). (b) Entropy variation *versus* temperature when a liquid is cooled towards absolute zero.

be coined as glass. The first has to do with the traditional ways of glass synthesis. According to this definition, glass is a solid and rigid material that is formed upon cooling from the liquid to the solid state, without the occurrence of any crystallization process.[1–3] The material becomes rigid since, during the cooling process, the viscosity increases. The second definition is based on structural criteria. Namely, it suggests that glass is an amorphous material in which there is no long-range order or periodicity in the way that constituent atoms are arranged.[1–3] Finally, a third definition considers thermal properties and states that glass is any hard material that exhibits a glass transition upon heating.[1–3] However, none of the above definitions is entirely complete. For instance, glasses can also be prepared from drying suitable gels, while all non-crystalline solids are not necessarily glasses. Thus, more thorough structural criteria are taken into consideration.

E. Stratakis

Dr Emmanuel Stratakis is a Research Director at the Institute of Electronic Structure and Laser (IESL) of the Foundation for Research and Technology-Hellas (FORTH), where he is leading the "Ultrafast Laser Micro- and Nano-processing" laboratory. He received his Ph.D. in Physics in 2001 from the University of Crete. He was a Visiting Scientist at the University of California Berkeley in the fall semesters of 2006 and 2008. He has over 220 publications and more than 8000 citations, h*-index = 48 (Scopus), and he has coordinated many National and EU grants. Since January 2020 he has been the founder and CEO of Biomimetic.*

It was Zachariasen (1932) who first tried to understand in structural terms how an inorganic oxide glass is formed. His primary observation was that glasses are formed from materials that are capable of forming three-dimensional networks.[1,2] In particular, he suggested the following four rules that have to be valid in order to achieve glass formation: i. every oxygen atom is linked at most to two other atoms, ii. the coordination number of all the other atoms must be small, iii. any polyhedra formed from the oxygen atoms which are around the other atoms, must share corners and not edges or faces, and iv. the polyhedra link up together in order to form a three dimensional network. Based on this guidance, Fig. 1a presents a schematic representation of the glass network for a typical sodium silicate glass, as proposed by Warren and Biscob.[4] Zachariasen's rules also provide a useful tool for predicting which oxides can form glasses and which cannot, as the aforementioned requirements can only be met by specific oxides. In particular, oxides that do form glasses must be of the type A_2O_3, AO_2 and A_2O_5. Typical examples are B_2O_3, P_2O_5, SiO_2 and GeO_2, for the formation of borate, phosphate, silicate and germanate glasses, respectively.

Following the definition of glass in terms of structural criteria, it is useful to consider it now from a thermodynamic point of view.[1–3] Fig. 1b shows schematically the variation of entropy (S) with temperature (T) when a liquid is cooled towards absolute zero. As the liquid is cooled there are two possible scenarios. Firstly, at a specific temperature crystallization may occur. Alternatively, in the case that the liquid is cooled very rapidly, crystallization may be avoided for the formation of glass. The case of crystallization is represented by a red line in Fig. 1b. When the liquid is cooled, it reaches a temperature at which crystals start to form. This temperature is marked as the melting temperature (T_m). Also, as the liquid crystallizes, it loses entropy, and the corresponding entropy loss is designated as the entropy of fusion ΔS_{fus}. The latter scenario involves rapid cooling of the liquid and is shown by

the blue line in Fig. 1b. In such a case, the crystallization at T_m is kinetically hindered, and instead of crystal formation below T_m, a super-cooled liquid is obtained that becomes more viscous as the temperature decreases. Eventually, for thermodynamic and kinetic reasons a glass transition temperature (T_g) is reached, where the super-cooled liquid transforms into a rigid solid, *i.e.* a glass, as shown by the green line in Fig. 1b. The exploitation of this transition between the super-cooled liquid and the rigid solid provides an amazing opportunity for the development of composite glasses upon incorporation of perovskite nanocrystals, two-dimensional materials, and metal nanoparticles.

The suitability of inorganic oxide glasses as hosts for the development of advanced optoelectronic and photonic platforms is prompted by several additional reasons. Firstly, inorganic oxide glasses are mostly fully transparent in the visible range. In addition, typical glasses are easy to fabricate from low-cost raw materials, while being stable, and of relatively low toxicity. Also, the optical, structural, and thermal properties of glasses are strongly related to their composition, and thus, can be easily modified. Based on the above, inorganic oxide glasses pose an ideal platform for hosting materials of unique optical and optoelectronic properties, towards boosting their potential use for advanced optoelectronic and photonic applications.

In the first part of the article, we present how inorganic oxide glasses have been outstanding hosting platforms for the incorporation of metal nanoparticles (NPs). The incorporation of metal particles inside glasses is motivated mainly by the ability to further tailor their optical properties by means of plasmon coupling and resonance effects that take place within the composite glasses. It is widely known that metal NPs exhibit extraordinary optical properties and functions when compared to the corresponding bulk metals.[5,6] In addition, parameters such as the particle shape, size and distribution have a significant influence on the resulting optical characteristics. Along these lines, we report on the fabrication procedures and the emerging application potentials of NP-based composite glasses, based on the induced optical properties upon NP encapsulation.

In the following part, we review the recent advancements in the field of composite perovskite-glasses (PV-glasses) in terms of the developed fabrication procedures and the resulting optoelectronic features, while considering the current limitations and challenges. In recent years organic and inorganic lead halide perovskites have gained enormous scientific attention due to their great potential for being the main component of next generation highly efficient photovoltaics.[7–9] Meanwhile their prominent role has also been demonstrated in a wide range of state-of-the-art photonic applications that include light-emitting diodes,[10–12] lasers,[13,14] photodetectors,[15–17] and black-light displays.[18] However, despite this remarkable evolution, there are two main factors that cause concerns over large-scale applicability and extensive commercial use. Namely, the poor stability of perovskite-based materials upon exposure to air and humidity and the significant toxicity of lead, which is the most widely used perovskite cation.[19–21] Regarding photonic applications, a promising strategy in order to overcome these important challenges is the encapsulation of perovskite nanocrystals (PNCs) within typical inorganic oxide glasses. Such an approach offers tremendous advantages in terms of improving the long term stability of the perovskite structures while minimizing the lead toxicity effects. Moreover, efficient tuning and enhancement of the photoluminescence properties of the PV-glasses are readily achieved by means of altering the morphology and composition of the embedded PNCs, as well as, by inducing plasmon interactions between the PNCs and the glass matrix. Thus, as motivated by the aforementioned factors, the development of advanced composite PV-glasses is a continuous scientific challenge, with promising outcomes towards next-generation optoelectronic and photonic applications.

In a similar manner, the embedment of two-dimensional (2D) materials inside transparent inorganic oxide glasses appears to be a promising strategy for the development of novel nanoheterojunctions in which controlled enhancement and tuning of the emission properties can be achieved. In the last part of this article, we review some typical examples of composite 2D material-glass architectures. Namely, we report on the fabrication procedures and the emerging application potentials, based on the induced optical properties upon encapsulating layers of 2D materials within glass matrices. Finally, the emerging perspectives of the three types of composite glass platforms towards advancing optoelectronic and photonic applications are summarized.

2. Composite glasses and related applications

2.1 Metal nanoparticle (NP) composite glasses

Small metal particles and nanoparticles (NPs) are widely researched due to the fact that they have different optical, dielectric and mechanical properties compared to their bulk counterparts. During the past years there has been a great amount of work concerning the study of composite glasses containing particles for both fundamental research studies and in view of their potential applications. Different parameters such as the particle shape and size, as well as, the distribution of the particles within the matrix strongly influence the properties of the composite glass. For instance, glasses containing particles such as silver and gold exhibit optical absorption in the visible range, the origin of which comes from the surface plasmon resonance (SPR) of the metal particles, while displaying third-order optical nonlinearity features.[22] As will become apparent in the following paragraphs, the synthesis of composite glasses with incorporated NPs is realized by means of a variety of routes that involve sol–gel methods, ion implantation, ion-exchange, and conventional melt-quench techniques.

The most studied composite glasses of this type are those containing silver nanoparticles (AgNPs). A great amount of scientific work has been made concerning their synthesis and properties towards advancing their potential use for various photonic applications (Table 1). This prominence is based on

Table 1 Summary of metal nanoparticle (NP) composite inorganic oxide glasses, along with brief details of the fabrication protocols, and key features of the optical properties

Study-year	Composite glass system	Synthesis protocol	Melting and annealing treatment	Key features and potential applications
Metal nanoparticle (NP) composite glasses				
Uchida *et al.*, 1994[22]	Ag/Cu in $50BaO–50P_2O_5/50CaO–50P_2O_5$	Conventional melt and heat-treatment	M: 490 °C A: 500 °C	NLO features
Hofmeister *et al.*, 1997[23]	Ag NPs–soda lime glass	Ion exchange procedure and electron beam irradiation	NR[a]	NLO features
Simo *et al.*, 2012[24]	Ag NPs–soda-lime silicate glass	Ion exchange procedure and annealing	M: 100–600 °C	Mechanism and kinetics of particle formation
Venkateswara *et al.*, 2015[25]	Ag NPs–$CaO–CaF_2–P_2O_5$ glass	Melt quenching technique and annealing	M: 550 °C	SPR peak position shifting
Yang *et al.*, 2009[26]	Ag NPs–soda-lime silicate glass	Ion exchange and annealing	M: 450/500 °C	3rd order NLO features
Pan *et al.*, 2003[27]	Ag NPs–SiO_2 glass	Sol–gel process and irradiation by ^{60}Co γ-ray and annealing	M: 550/650/750 °C	SPR peak position shifting
Venkateswara *et al.*, 2014[28]	Ag NPs–calcium phosphate glass	Melt quenching technique and annealing	M: 550 °C	NLO features
Som *et al.*, 2009[29]	Er^{3+}: Au NPs–$K_2O–B_2O_3–Sb_2O_3$ glass	Melt quenching technique and annealing	M: 260 °C	In upconversion-based optical devices due to high green emission and red fluorescence of very high intensity
Soltani *et al.*, 2016[30]	Er^{3+}: Ag NPs–phosphate glasses	Melt quenching technique and annealing	M: 503 °C	NLO features
Soltani *et al.*, 2016[31]	Er^{3+}: Ag NPs–phosphate glasses	Melt quenching technique and annealing	M: 503 °C	Promising host materials for 1.53 μm broad band amplification
Soltani *et al.*, 2018[32]	Er^{3+}/Yb^{3+}: Ag NPs phosphate glasses	Melt quenching technique and annealing	M: 250 °C	Potential material for solid state lasers
Nurhafizah *et al.*, 2016[33]	Er^{3+}/Nd^{3+}: Ag NP lithium niobate tellurite glass	Melt quenching technique and annealing	M: 320 °C	Self-cleaning glass application
Haouari *et al.*, 2018[34]	Eu^{3+}: Ag NPs tellurite glass	Melt quenching technique and annealing	M: 340 °C	Eu^{3+} quenching emission
Zmojda *et al.*, 2018[35]	Eu^{3+}: Ag NPs antimony germanate borate glass	Melt quenching technique and annealing	M: 300 °C	In SERS substrates and biophotonic devices
Vijayakumar *et al.*, 2016[36]	Eu^{3+}: Ag NPs borophosphate glasses	Melt quenching technique and annealing	M: 390 °C	Active medium for laser
Hua *et al.*, 2018[37]	Dy^{3+}: Ag NPs tellurite glasses	Melt quenching technique and annealing	M: 320 °C	Potential for lighting devices because of the tunable white fluorescence
Lakshminarayana *et al.*, 2009[38]	Pr^{3+}: Ag NPs $TeO_2–ZnO–Nb_2O_5–MoO_3$ glasses	Melt quenching technique and annealing	M: 350 °C	Pr^{3+} luminescence enhancement
Machado *et al.*, 2020[39]	Te particles-antimony sodium polyphosphate glass	Melt quenching technique and annealing	M: 430 °C	Refractive index variation
Halimah *et al.*, 2019[40]	Er NPs-bio-silica borotellurite glass containg silver oxide	Melt quenching technique and annealing	M: 400 °C	Gain media for solid state lasers
Machado *et al.*, 2019[41]	$Er^{3+}/Yb^{3+}/Ce^{3+}$: Cu NPs tellurite glasses	Melt quenching technique and annealing	M: 280 °C	Infrared optical devices
Podlipensky *et al.*, 2004[42]	Ag NPs–soda-lime glass	Ion exchange and annealing/thermal poling	M: °C	Optical and optoelectronic elements
Sasai *et al.*, 2001[43]	Au NPs–borate glass	Melt quenching technique and annealing	M: 450 °C	NLO features
Singla, *et al.*, 2020[44]	Au NPs–bismuth borate glass	Melt quenching technique and annealing	M: 350 °C	With increasing nonlinear refractive index, suitable for optical devices
Konidakis *et al.*, 2018[45]	$xAgI-(1-x)AgPO_3$	Melt quenching technique	M: 450 °C	Second harmonic generation (SHG)/optical switches, optical modulator devices
Konidakis *et al.*, 2012[46]	$AgPO_3$/silica PCF	PCF infiltration	M: 450 °C	Photosensitive PBG guidance/photonic crystal fibers
Konidakis *et al.*, 2014[47]	$xAgI-(1-x)AgPO_3$/silica PCS	PCF infiltration	M: 450 °C	AgNPs tunable PBG guidance/photonic crystal fibers

[a] NR stands for not reported.

the opportunity of tuning the silver surface plasmon resonance (SPR) peak wavelength from 400 to 530 nm, upon changing the particle size and the local refractive index near the particle surface. Hofmeister *et al.* reported a path for the formation of AgNPs in a soda-lime glass matrix, in which the ion-exchange route is followed while the samples are irradiated by an electron beam.[23] The findings of this work showed a high concentration of AgNPs, while at the same time a narrow particle size distribution and homogeneity in their arrangement was obtained. More importantly, when compared to conventional thermal treatments of the glass substrates, the employment of an electron beam is less time consuming while offering significantly higher reproducibility. Rather differently, Simo *et al.* applied thermal treatment in order to study the formation mechanism of silver NPs inside a soda-lime silicate glass by means of ion-exchange.[24] The conclusions of this work showed that both the growth and the size of the particles strongly depend on the glass intrinsic reduction mechanisms. Also, for the particles to be created the first step is the formation of dimers, which grow with the addition of silver as the annealing time increases.[24]

Since the particle size depends on the annealing conditions as noted above, one might expect that the optical, electrical, and mechanical properties of the composite glasses will change accordingly. Along these lines, Rao *et al.* explored these changes for a calcium fluorophosphate glass system with AgNPs embedded.[25] It was demonstrated that by increasing the time of thermal treatment there is an increase in the hardness and density of the glass. Meanwhile a decrease in brittleness is observed, while the AgNP particle size increases. As a consequence, a redshift in the SPR peak wavelength is observed, accompanied by an increase in the full width half maximum (FWHM). Going on further, Yang *et al.* explored the third-order optical nonlinearity and ultrafast dynamics of silicate glasses containing AgNPs, by changing the temperature of the annealing process rather than the time.[26] Notably, by increasing the thermal treatment temperature an increase of the third-order susceptibility was obtained, while at the same time there was an acceleration of the fast decay process and the corresponding amplitude ratio. These findings were attributed to the enhancement of electron–phonon coupling phenomena within the glass matrix.

Pan *et al.* studied the formation of mesoporous SiO_2 glasses containing silver particles.[27] For the sake of comparison, some of the particles were irradiated by a ^{60}Co γ-ray source, while others were not. The irradiated samples were subjected to heat treatment at different temperatures, while the non-irradiated samples underwent the same thermal treatment. Absorption spectra exhibited a reversible peak shift effect of the SPR with the variation of the particle size. Venkateswara *et al.* synthesized calcium phosphate glasses with embedded AgNPs.[28] For the nanoparticle formation within the glass heat treatments of different durations were implemented. In agreement with other studies, the authors reported the expected SPR redshift upon NP size enhancement, as well as, an increase in the glass hardness and a decrease in brittleness.

The next category of composite glasses with embedded AgNPs are the ones containing rare earth ions such as Er^{3+}, Pr^{3+}, Dy^{3+}, *etc.* (Table 1). Glasses in which there is a coupling between metal particles and rare-earth ions offer a variety of modifications in both structural and optical properties. Based on the literature, the most studied rare-earth ion to date is Er^{3+}, mainly because it offers both green and red emission characteristics. This feature renders Er^{3+} containing composite glasses potential candidates for advanced optical devices.[29] The synthetic methods for this type of glass are similar to the ones mentioned above for AgNP composite glasses. Soltani *et al.* demonstrated the development of phosphate glasses containing spherical AgNPs, as well as, Er^{3+} ions.[30] From both Raman and FTIR spectra it was revealed that AgNPs influence the phosphate backbone of the network, by causing its partial depolymerization. Moreover, it was noted that the optical band gap decreases, due to the increase of the non-bridging oxygens as the silver NPs grow in size. In a later study of the same glass system, the authors reported that the presence of AgNPs has an impact on the intensity of fluorescence (Fig. 2a), and also on the lifetime of the Er^{3+} ion transition $^4I_{13/2} \rightarrow {}^4I_{15/2}$.[31] The first observation was ascribed to the local field enhancement induced by SPR of AgNPs, whereas the second was attributed to the energy transfer between Er^{3+} ions and AgNPs. Along these lines, the next step was to consider a AgNP composite glass with at least two rare-earth ions inside the matrix. Soltani *et al.* reported on the synthesis of co-doped Er^{3+}/Yb^{3+} phosphate glass containing AgNPs.[32] The fluorescence was studied and an increase was observed as the NP size was increased. Such findings were attributed to the SPR effect of AgNPs on the local electric field around the ions. Another indicative system containing two different rare-earth ions was studied by Nurhafizah *et al.*,[33] in which the self-cleaning properties of the glass were investigated. The glass synthesized was a LNT glass containing AgNPs and Er^{3+}/Nd^{3+} ions. Impressively, higher water contact angles were obtained as the AgNP size increased, indicating that the glass surface becomes more hydrophobic.

There are additional works in which the glass matrices are doped with other rare-earth ions, such as Eu^{3+}, Dy^{3+} and Pr^{3+}. From these rare-earth ions the most examined in the literature is Eu^{3+}. Haouari *et al.* explored the synthesis and characterization of tellurite glasses containing AgNPs doped with Eu^{3+} ions.[34] The obtained samples were heat treated at the same temperature but for different periods. The most interesting result of this work is that there is an enhancement in the luminescence of Eu^{3+} due to the surface plasmon resonance of the AgNPs inside the glass matrix. Fig. 2b presents the indicative energy level diagram showing the different processes involved in the obtained emission of Eu^{3+} ions and AgNPs, while Fig. 2c depicts the chromaticity coordinates of the Eu^{3+} glasses with and without AgNPs. Going on further, Zmojda *et al.* presented the synthesis of antimony borogermanate-based glasses which contain the same NPs and ions as the previous work.[35] The conclusion of this study shows that there is an increase of 36% in the emission at 616 nm as the time of the annealing procedure increases. The authors also proposed

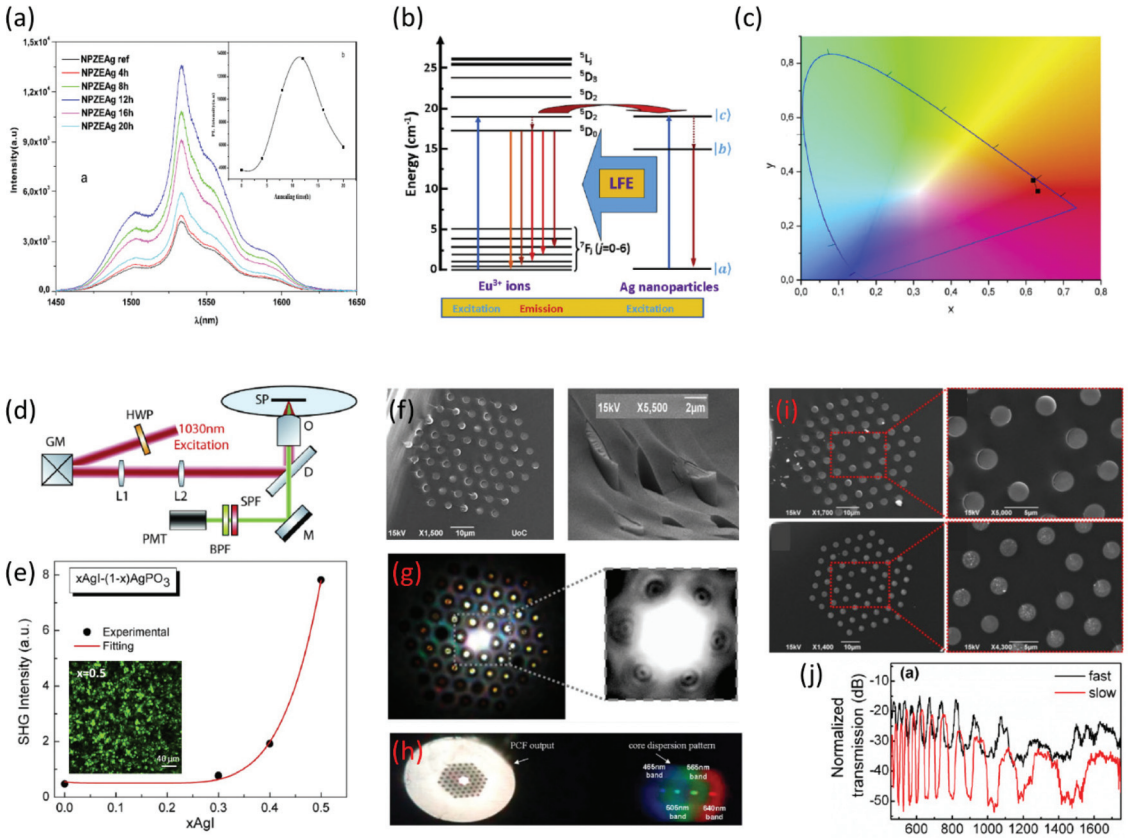

Fig. 2 (a) PL intensity relative to $^4I_{13/2} \rightarrow {}^4I_{15/2}$ transition. The inset shows the effect of the annealing time on the PL intensity (a has been reproduced from ref. 31 with permission from Elsevier, copyright 2016). (b) Energy level diagram showing the different processes involved in the emission of Eu^{3+} ions and AgNPs. (c) Chromaticity coordinates of the Eu^{3+} glasses with and without AgNPs (b and c have been reproduced from ref. 34 with permission from Elsevier, copyright 2018). (d) Schematic representation of the second harmonic generation (SHG) imaging microscopy experimental setup. (e) SHG signal intensity for *x*AgI-(1 − *x*)$AgPO_3$ glasses. The inset presents an indicative SHG photo under a microscope (d and e have been reproduced from ref. 45 with permission from Elsevier, copyright 2018). (f) Scanning electron microscopy (SEM) scans of the cleaved end face of an infiltrated photonic crystal fiber (PCF) with glass. (g) Light fine feature modes at the PCF end face propagating through $AgPO_3$ glass strands. (h) White-light far field diffraction pattern outcoupled from the $AgPO_3$/silica PCF projected through a phase mask (f–h have been reproduced from ref. 46 with permission from Optica Publishing Group, copyright 2012). (i) SEM scans of the cleaved end face of an infiltrated PCF fiber *via* fast-cooling (upper part) and slow-cooling (lower part) procedures. (j) Transmission spectra of 1 cm long *x*AgI-(1 − *x*)$AgPO_3$/PCF fabricated *via* fast-cooling and slow-cooling methods (i and j have been reproduced from ref. 47 with permission from MDPI, copyright 2014). All content has been reproduced by permission.

a bottom-up approach for the synthesis of AgNPs on glass fibers, based on the reduction of Ag^+ cations from the inside part of the glass towards the surface. It has to be mentioned that the concentration of silver ions plays an important role in this process, as for low concentrations there were AuNPs observed on the surface of the developed fibers.[35] Vijayakumar *et al.* reported on borophosphate glasses containing AgNPs as before, while being doped with Eu^{3+} ions.[36] The obtained emission features revealed an enhancement in the luminescence intensity, while the composite glasses were capable of emitting red light by 405 nm excitement. The later finding renders them suitable active media for solid state lasers. Moving on to another dopant, Pr^{3+}, Hua *et al.* incorporated it in tellurite glasses containing AgNPs.[37] Similarly to other studies, the authors found an enhancement in the intensity of the luminescence at 493 nm. Finally, Lakshminarayana *et al.* synthesized AgNPs containing tellurite-based glasses in which Dy^{3+} ions were incorporated.[38] Notably, the presence of AgNPs induces a 29% increase in the luminescence intensity.

Machado *et al.* investigated the synthesis and properties of antimony sodium polyphosphate glasses containing tellurium particles. The particle production consists of a reduction reaction that transforms Te^{4+} into Te^0.[39] Depending on the concentration of antimony oxide the concentration of Te particles also changes, which leads to the change of glass color. Namely, for low concentrations the authors obtained a minimal amount of Te particles and the sample remained colorless, whereas for higher concentrations the glass switched to black. Halimah *et al.* reported on the synthesis and optical characterization of an erbium NP doped silica borotellurite bioactive glass system containing silver oxide.[40] The promising results of this work showed that this type of glass could be

used as gain medium for solid state lasers. Going on further, Machado *et al.* reported the synthesis of co-doped $Er^{3+}/Yb^{3+}/Ce^{3+}$ tellurite glasses containing copper (Cu) NPs.[41] The effect of the NPs on the optical properties was investigated, and it was revealed that Cu NPs enhanced the Er^{3+} emission by 47%. Also, a 50% increase was noted in the lifetime of the transition $^4I_{13/2} \rightarrow {}^4I_{15/2}$. These findings supported the conclusion that there is a possibility of population inversion within the glass system, which can render the composite glasses of this family potential candidates for lasing applications.

Since by now we have considered the formation of inorganic oxide glasses containing AgNPs along with their optical properties, it is interesting to mention that there is a way for demolishing and dissolving AgNPs within glasses into Ag^+ cations. Indicatively, Podlipensky *et al.* employed thermal poling on a soda-lime glass containing Ag nanoparticles near the surface region.[42] After subjecting the sample to an electric field while being heat treated, the bleaching of the sample was observed, which was attributed to the dissolution of AgNPs to silver cations, Ag^+. Moreover, it was reported that if the processed sample was further annealed, there was a restoration of AgNPs. Notably, the glass remains intact throughout thermal poling and annealing treatments.

As mentioned above, glasses containing metal NPs have different linear, as well as nonlinear (NLO) optical properties. There is a great amount of work dedicated to exploring the optical properties of these types of materials. At this point, we are going to focus on glasses with embedded gold (Au) particles. The work by Sasai *et al.* includes the relaxation behavior investigation of NLO properties of borate glasses with incorporated Au NPs.[43] The authors showed that there is a direct correlation between particle size and the electron–phonon coupling constant, *i.e.* by increasing the size the constant decreases. Also, upon increasing the size the tail component of the decay curve increases. These observations indicate that the relaxation times are dependent on the particle size. Singla *et al.* investigated the optical properties of bismuth borate glasses containing Au NPs of different sizes.[44] Namely, it was revealed that as the particle size increases there is an increase in the refractive index and nonlinear refractive index, whereas there is a decrease in the nonlinear absorption coefficient. Along similar lines, Konidakis *et al.*,[45] employed nonlinear laser imaging microscopy to explicitly study the effect of glass composition and temperature on the second harmonic generation (SHG) in a series of xAgI-$(1-x)$$AgPO_3$ silver-rich phosphate glasses (Table 1). Fig. 2d presents a schematic animation of the SHG imaging experimental setup. It was revealed that the SHG intensity increased nonlinearly with AgI content (Fig. 2e). Such an observation was attributed to the agglomeration of AgNPs upon increasing x, and thus, to the formation of larger silver clusters within the phosphate glass. Based on the above studies, such glass systems are of great interest and show potential for low-cost optical switches, electro-optic filters, and optical modulator devices.

Finally, metal NP containing glasses were also explored in the field of photonic crystal fibers (PCFs), towards advancing photonic features and related applications (Table 1).[46,47] Konidakis *et al.* reported on the development of an all-glass, photosensitive, $AgPO_3$/silica photonic bandgap (PBG) fiber, upon infiltrating the capillaries of a commercially available PCF with $AgPO_3$ glass.[46] Fig. 2f depicts the SEM scans of the cleaved end face of the infiltrated PCF, in which the $AgPO_3$ glass strands are visible exceeding the end face, while Fig. 2g shows the fine-featured modes of light at the PCF end face propagating through the $AgPO_3$ strands. The incorporation of the phosphate glass induces PBG guidance in the range between 350 and 1650 nm of the transmission profile.[46] Fig. 2h presents the corresponding white-light far field diffraction pattern, outcoupled from the $AgPO_3$/silica PCF and projected through a phase mask. More interestingly, in a later study the same authors demonstrated the optical spectral tuning of similar all-glass PBG fibers.[47] It was shown that upon changing the PCF infiltration conditions it was possible to tune the waveguiding features of the composite fibers. In particular, when the all-glass $AgPO_3$/silica photonic bandgap (PBG) fiber was prepared by a slow-cooling protocol, instead of the typical fast-cooling procedure, silver particle agglomeration was noticed inside the phosphate strands (Fig. 2i). The formation of larger silver-based clusters had an immediate effect on the transmission characteristics of the composite fibers (Fig. 2j). Namely, the extinction ratio of the transmission stop-bands increases from 15 to 30 dB cm^{-1}, while a FWHM broadening of the discrete spectral stopbands was also noticed.

2.2 Perovskite composite glasses

To date three main methods have been developed for the synthesis of composite perovskite-glasses (PV-glasses). Fig. 3 depicts schematically all three of them. According to the first and most popular one, both glass and perovskite powder precursors are mixed and melted together within the same crucible. Based on this pre-melting mixing procedure, the perovskite precursors are located inside the glass after the initial quenching. Following this, the perovskite crystallization is achieved in a second stage by means of additional annealing procedures at high temperatures, often exceeding 800 °C. Along similar lines, the second synthesis route involves the same initial mixing of all precursors before melting. However, after glass quenching, prior to typical heating protocols for crystallization, the perovskite formation is first induced by means of laser irradiation. After this laser-assisted (LA) initiation step the crystallization is finalized upon conventional thermal treatment. Rather differently, according to the third fabrication procedure, the perovskite precursors are not added prior to glass melting. Instead, a pristine inorganic oxide glass is firstly prepared by typical quenching. After this, separately pre-synthesized perovskite nanocrystals (PNCs) are embedded within the glass in a controlled manner. The PV-glasses of this section will be categorized according to the fabrication protocols, while the advantages and limitations of every technique will be discussed. Table 2 summarizes the fabricated PV-glass systems, while including the main synthesis parameters and the key features of the optical properties.

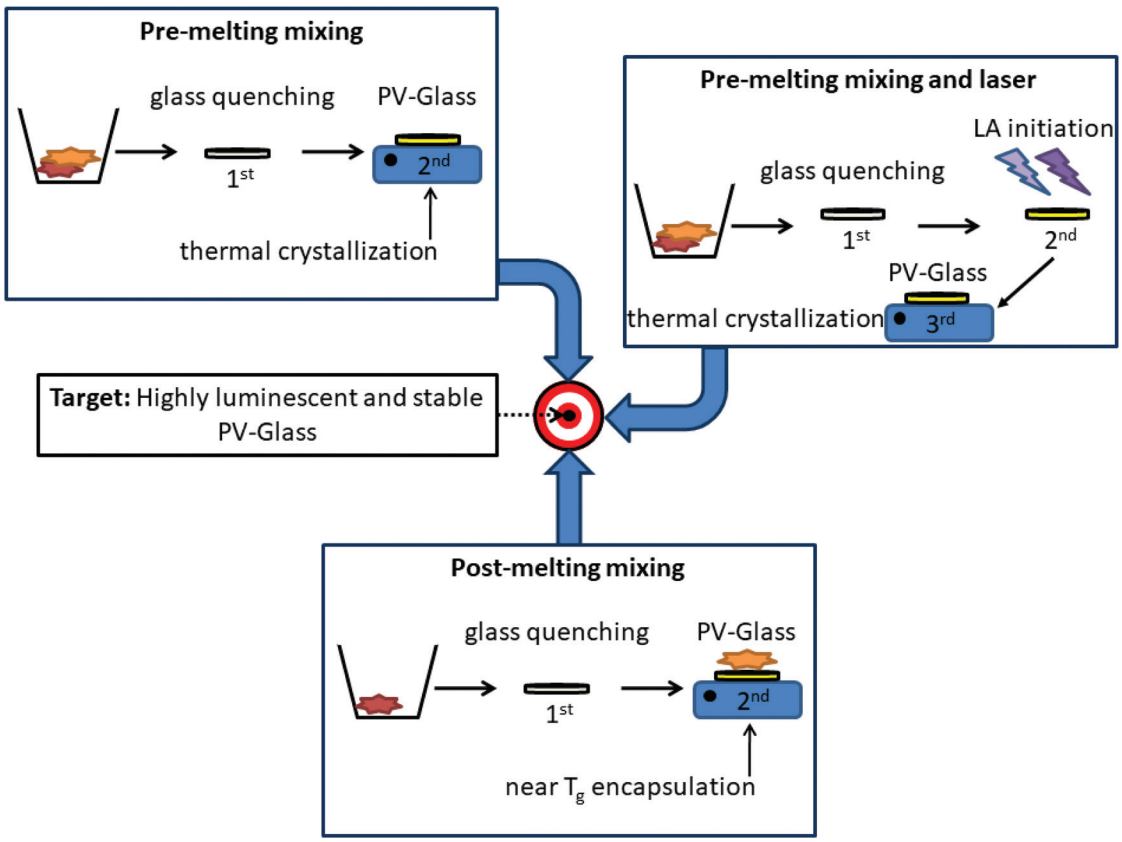

Fig. 3 Schematic representation of the developed procedures for the synthesis of composite perovskite glasses (PV-glasses).

2.2.1 Perovskite-glasses by total precursor melting. We consider first PV-glasses synthesized upon following typical pre-melting encapsulations. The most common glass family for this synthesis route is the borosilicates.[48–63] The popularity of borosilicate glasses as perovskite hosts is prompted by their relatively high glass transition temperatures that facilitate post-glass melting annealing treatments at temperatures within the range of 400–1200 °C (Table 2). For instance, Li *et al.* reported the formation of $CsPb_2Br_5$ quantum dots (QDs) within a borosilicate-based glass matrix under various heat treatments.[48] Boron and silicate components form most of the glass network (72%), while small fractions of Al_2O_3 (5%) and ZnO (9%) are added as additional network former components. Both glass and perovskite precursors were mixed and melted simultaneously at 1200 °C for 30 min. Following the initial melting, further annealing treatments were performed at temperatures close to T_g, *i.e.* at 410 °C for 10 hours, in order to achieve perovskite growth. PV-glasses of this study exhibit photoluminescence features at the vicinity of 510 nm, induced by the formation of $CsPb_2Br_5$ QDs of an average diameter of around 4 nm. Based on this, in a later study,[49] Li *et al.* demonstrated the realization of a white light emitting diode (WLED) by combining InGaN blue chips, red phosphors, and the so-formed $CsPb_2Br_5$ QD borosilicate glass. Similarly, Yang *et al.* developed a WLED based on the synthesized green emitting borosilicate encapsulated $CsPbBr_3/Cs_4PbBr_6$ QDs, a red phosphor, and a blue chip.[57]

Interestingly enough, the emission properties of the composite PV-glasses are readily tuned in accordance with the type of the encapsulated PNCs. Indeed, it is well known that the modification of the halide anion changes the interatomic distance and angle of the X–B–X bonds within the BX_6 octahedra of the perovskite lattice. For instance, in the case of all-inorganic lead halide perovskites, the energy bandgap progressively decreases from Cl to Br to I, thus the PL profile shifts to higher wavelengths.[12,64–66] Based on this, Liu *et al.* demonstrated the formation and tunable emission of cesium lead halide perovskite $CsPbI_xBr_{3-x}$ QDs in borosilicate glasses.[50] Namely, by changing the molar ratios of halide precursors a tunable photoluminescence from 520 nm to 698 nm was observed. The developed PV-glasses exhibit high luminescence intensity, and narrow PL emission as the corresponding $CsPbX_3$ QD solutions (Fig. 4a). Moreover, outstanding PL stability maintaining 95.8% of its initial light-converting efficiency following 500 h of accelerated aging at high temperature and high humidity is also shown.[50] Along similar lines, Chen *et al.* reported on the full-spectral tunable emissions of PV-glasses upon altering the halogen ion of $CsPbX_3$ QDs within a borophosphate-based matrix.[67] Fig. 4b shows the representative PL spectra of the developed glasses upon excitation at 345 nm, along with photos of the perovskite powders and composite glass fragments under UV lamp irradiation. The encapsulation of QDs within glasses resulted in considerable improvement of

Table 2 Summary of the developed perovskite–glasses (PV–glasses), fabrication protocols, and key features of the optical properties

Study-year	PV–glass system	Synthesis protocol	Melting and annealing treatment	Demonstrated PL stability	Key features/embedded PL patterns
Synthesis route: total precursor melting					
Li *et al.*, 2017[48]	$CsPb_2Br_5$/borosilicate	Total precursors melting – random PNC positioning	M:1200 °C, 30 min A: 360 °C, 2 h	NR[a]	—/No
Li *et al.*, 2018[49]	$CsPb_2Br_5$/borosilicate	Total precursors melting – random PNC positioning	M:1200 °C, 30 min A: 360 °C, 3–10 h	NR[a]	WLED/no
Liu *et al.*, 2018[50]	$CsPbI_xB_{3-x}$/borosilicate	Total precursor melting – random PNC positioning	M: 1200 °C, 10 min A: 520 °C, NR[a]	85 °C, 85% RH, 500 h 95.8% PL intensity	—/No
Liu *et al.*, 2018[51]	$CsPbI_3$/zinc borosilicate	Total precursor melting – random PNC positioning	M: 1200 °C, 10 min A: 480–560 °C, 10 h	150 °C, 200 h 91.1% PL intensity	—/No
Liu *et al.*, 2019[52]	Sn-Doped $CsPbBr_3$ ($CsPb_{1-x}Sn_xBr_3$)/ borosilicate	Total precursor melting – random PNC positioning	M: 1200 °C, 10 min A: 450–550 °C, 5 h	85% RH, 100 d, stable 150 °C, 100 h ~90% PL intensity	WLED/No
Xu *et al.*, 2019[53]	$CsPbBr_3$/AgNPs borosilicate	Total precursor melting – random PNC positioning	M: 1200 °C, 10 min A: 450–650 °C, 5 h	NR[a]	5 fold PL enhancement/ No
He *et al.*, 2019[54]	Mn^{2+} doped $CsPbBr_xI_{3-x}$/zinc borosilicate	Total precursor melting – random PNC positioning	M: A: 520 °C, 10 h	air, 70 d 84% PL intensity	WLED/No
Zhu *et al.*, 2020[55]	$CsPbBr_3$: xBi^{3+}/borosilicate	Total precursor melting – random PNC positioning	M: 900 °C	Thermal stability	—/No
Jin *et al.*, 2020[56]	$CsPbX_3$ (X = Cl/Br, Br)/borosilicate	Total precursor melting – random PNC positioning	M: A: 470–530 °C, 10 h	500 °C, ~90% PL intensity Water, 75 d, stable	—/No
Yang *et al.*, 2020[57]	$CsPbBr_3$, Cs_4PbBr_6/borosilicate	Total precursor melting – random PNC positioning	M: 1150–1200 °C, 5–30 min A: 420–560 °C, 10 h.	Xenon lamp irradiation, 500 W, 10 h, 61% of the original PL intensity Water, 70 h, stable	WLED/No
Zhao *et al.*, 2020[58]	Cd^{2+} doped $CsPbBr_3$/borosilicate	Total precursor melting – random PNC positioning	M: 1200 °C, 20 min A: 500 °C, 10 h	Water, 60 d, 84.6% PL intensity	WLED/no
Zhang *et al.*, 2020[59]	Tb^{3+} doped $CsPbI_3$/borosilicate	Total precursor melting – random PNC positioning	M: 1100 °C, 10 min A: 480–540 °C, 10 h	Water, 60 d, 89.8% PL intensity	—/No
Zheng *et al.*, 2020[60]	$CsPbBr_3$/Cs_4PbBr_6/borosilicate	Total precursor melting – random PNC positioning	M: 1150 °C, 5 min A: 420–4600 °C, 1–10 h	85 °C, 85% RH, 110 h 80% PL intensity Xenon lamp irradiation, 500 W, 110 h, 45% of the original PL intensity	LED/No
Zhang *et al.*, 2020[61]	$CsPbCl_3$: $CsPbI_3$/zinc borosilicate	Total precursor melting – random PNC positioning	M: 1200 °C, 10 min A: 440–560 °C, 10 h	Water, 60 d, 95% PL intensity 4 heating/cooling cycles at 200 °C, >80% PL intensity	$CsPbCl_3$: $CsPbI_3$ coexistence, WLED/no
Liu *et al.*, 2021[62]	$CsPbCl_2Br_1$/borosilicate	Total precursor melting – random PNC positioning	M: 1200 °C, 30 min A: 440 to 530 °C, 10 h	NR[a]	—/No
Xu *et al.*, 2021[63]	$CsPbBr_3$/borosilicate	Total precursor melting – random PNC positioning	M: 1100 °C, 30 min, A: 430–490 °C for 10 h	NR[a]	—/No
Chen *et al.*, 2018[67]	$CsPbX_3$ (X = Cl, Br, I)/$CsPbCl_mBr_{3-m}$/ Zn–P–B–Sb based	Total precursor melting – random PNC positioning	M: 800 °C, 20 min A: 300–400 °C, 2 h	Water, 30 d, 70% PL intensity Heating/cooling cycles (150–200 °C), 70–80% PL intensity	LED/No

Table 2 *(Contd.)*

Study-year	PV–glass system	Synthesis protocol	Melting and annealing treatment	Demonstrated PL stability	Key features/embedded PL patterns
Yang *et al.*, 2022[68]	$CsPbBr_3$/borosilicate	Total precursor melting – random PNC positioning	M: 1200 °C, 15 min A: 480–500 °C, 10 h	80 °C, 360 h, 80% PL intensity Water, 360 h, 90% PL intensity Heating/cooling cycles (303–468 K), stable PL intensity UV light, 368 h, 88% PL intensity	WLED device/No
Liu *et al.*, 2019[69]	$CsPbCl_xBr_{3-x}$ (x = 0, 1, 1.5, 2, and 3)/ borosilicate	Total precursor melting – random PNC positioning	M: 1250 °C, 10 min A: 450 °C, 5 h	85 °C, 85% RH, 100 h 92.4% PL intensity Heating/cooling cycles (400–450 K), 95,2% and 86.3% PL intensity	LED indoor plant growth/ No
Xu *et al.*, 2021[70]	$CsPbBr_3$/borosilicate	Total precursor melting – random PNC positioning	M: 1150 °C, 10 min A: 450–490 °C, 10 h	Water, 2 weeks, 83% initial PL intensity Heating/cooling cycle (250 °C), stable PL intensity	X-ray scintillators/No
Wang *et al.*, 2020[71]	$CsPb(Cl,Br)_3$/borate	Total precursor melting – random PNC positioning	M: 1000 °C, 30 min A: 470/520 °C, 1 h	NR[a]	X-ray scintillators/No
Niu *et al.*, 2021[72]	$CsPbBr_3$/tellurite	Total precursor melting – random PNC positioning	M: 800 °C, 10 min A: 450–600 °C, 10 h	Heating/cooling cycles (up to 200 °C)	X-ray scintillators/no
Lu *et al.*, 2021[73]	$CsPbBr_3$/glass	Total precursor melting – random PNC positioning	M: 800 °C, 10 min A: 450–500 °C, 8 h	NR[a]	10 fold PL enhancement/ No
Zhang *et al.*, 2020[74]	$CsPbBr_3$/borosilicate	Total precursor melting – random PNC positioning	M: 1200 °C, 15 min A: 475 °C, for 5 h	8 heating/cooling cycles (413 K), stable PL intensity	—/No
Duan *et al.*, 2021[75]	Cs_4PbBr_6/borosilicate	Total precursor melting – random PNC positioning	M: 1200 °C, 10 min A: 450–550 °C, 5 h	NR[a]	Switchable PL/No
Ye *et al.*, 2019[76]	$CsPbCl_{3-x}Br_x$, $CsPbBr_3$, $CsPbBr_{3-x}I_x$, $CsPbI_3$/borogermanate	Total precursor melting – random PNC positioning	M: 1200 °C, 30 min A: 440–500 °C, 10 h	heating/cooling cycle (200 °C), stable PL intensity Water, 1 week, stable PL	LED device/No
Zhou *et al.*, 2020[77]	Mn doped $CsPbCl_3$, $CsPb(Cl/Br)_3$/ germanate	Total precursor melting – random PNC positioning	M: 1380 °C, 20 min A: 460–500 °C, 10 h	NR[a]	—/No
Yuan *et al.*, 2018[78]	$CsPbBr_3$/borotellurite	Total precursor melting – random PNC positioning	M: 550–950 °C, 30 min A: 200–400 °C, 2–12 h	Heating/cooling cycles (100, 150, 200 °C) 60–70% PL intensity Water, 45 d, 60% PL intensity	WLED device/No
Liu *et al.*, 2019[79]	$CsPbBr_3$/Yb/Ln (Ln = Er, Tm/ borotellurite	Total precursor melting – random PNC positioning	M: 800 °C, 30 min A: 350 °C, 2 h	Water, 30 d, 95% PL intensity	—/No
Erol *et al.*, 2020[81]	$CsPbBr_3$/tellurite	Total precursor melting – random PNC positioning	M: 800 °C, 30 min A: 310–370 °C, 1–7 h	75 °C, 40% PL intensity Water, 60 d, stable	LED device/no
Ai *et al.*, 2016[82]	$CsPbBr_3$/phosphate	Total precursor melting – random PNC positioning	M: 1050 °C, 20 min A: 380–430 °C, 2–10 h	NR[a]	—/No
Di *et al.*, 2017[83]	$CsPbBr_3$/phosphosilicate	Total precursor melting – random PNC positioning	M: — A: 380–450 °C, for 10 h	125 °C, 63% PL intensity UV light, 6 d, 85% of the initial intensity	WLED device/No
Chen *et al.*, 2018[84]	$CsPbBr_3$, $CsPbI_3$/phosphosilicate	Total precursor melting – random PNC positioning	M: 700 °C, 20 min A: 300 °C, for 2–10 h	Heating/cooling cycles (150, 200 °C), 75% PL intensity	WLED device/No
Chen, 2019[85]	$CsPbCl_3$/phosphate	Total precursor melting – random PNC positioning	M: 1050 °C, 25 min A: 380–420 °C, for 10 h	—	—/No
Li *et al.*, 2020[86]	$CsPbBr_3$/phosphate	Total precursor melting – random PNC positioning	M: 650 °C, 20 min A: —	Heating/cooling cycle (210 °C), stable PL intensity Water, 50 d, stable	Mechanical-hydration growth/no

Table 2 *(Contd.)*

Study-year	PV–glass system	Synthesis protocol	Melting and annealing treatment	Demonstrated PL stability	Key features/embedded PL patterns
Li *et al.*, 2020[87]	$CsPbX_3$ (X = Cl, Br, I)/lead-phosphate	Total precursor melting – random PNC positioning	M: 650 °C, 20 min A: 300–340 °C, for 2 h	NR[a]	—/No
Wang *et al.*, 2020[88]	$CsPbX_3$ (X = Cl, Br, I)/ fluorophosphate	Total precursor melting – random PNC positioning	M: 900 °C, 20 min Humidity chamber: 70%, 30 min	NR[a]	Hydration growth/No
Weng *et al.*, 2020[89]	α-$CsPbI_3$/Sb_2S_3-based chalcogenide	Total precursor melting – random PNC positioning	M: 920 °C, 10 h A: 277–310 °C, for 20 h	NR[a]	—/No
Synthesis route: total melting and laser-assisted procedures					
Huang *et al.*, 2020[97]	$CsPbBr_3$/borosilicate	Total precursor melting – fs laser-assisted growth – annealing treatment	M: 1100 °C, 20 min LA: 800 nm, 97.74 kW cm^{-2} A: 350 °C, 5 h	Water and ethanol, 30 d, stable PL intensity	Switchable PL/Yes
Huang *et al.*, 2020[98]	$CsPb(Cl/Br)_3$/borosilicate	Total precursor melting – fs laser-assisted growth – annealing treatment	M: 1100 °C, 20 min LA: 800 nm, 97.74 kW cm^{-2} A: 350 °C 5 h	Water, 30 d, stable PL intensity	Switchable PL/Yes
Hu *et al.*, 2020[99]	$CsPbBr_3$/borogermanate	Total precursor melting – fs laser-assisted growth – annealing treatment	M: 1200 °C, 30 min LA: A: 400 °C, 5 h	NR[a]	Enhanced QE/laser written lines
Du *et al.*, 2020[100]	$CsPbBr_3$/borophosphate	Total precursor melting – fs laser-assisted growth – annealing treatment	M: 900 °C, 30 min A: 430 °C, for 3–12 h LA: 351/532/800/1064 nm nanosecond laser HT: 350 °C, for 12 h	Heating/cooling cycles (117, 227 °C), stable PL intensity Water, 10 d, 90% PL intensity	—/No
Synthesis route: post-melting encapsulation					
Shinozaki *et al.*, 2020[102]	$(C_6H_5C_2H_4NH_3)_2PbBr_4$/borosilicate	Post-melting encapsulation– solvent evaporation	M: 450 °C, 4 h SE: 100 °C, 30 min	NR[a]	—/No
Kawano *et al.*, 2020[103]	$(C_6H_5C_2H_4NH_3)_2PbBr_4$/borosilicate	Post-melting encapsulation–solvent evaporation	M: 450 °C, 4 h SE: 100 °C, 30 min	NR[a]	—/No
Konidakis *et al.*, 2020[104]	$CsPbBr_3$/phosphate	Post-melting, cw laser-assisted, no annealing	M: 450 °C, 30 min LA: 1.6 W, 100 ms, cw 455 nm A: 160 °C	Ambient air, 60 days	Cw laser processing/ Microdotted patterns

[a] NR stands for not reported.

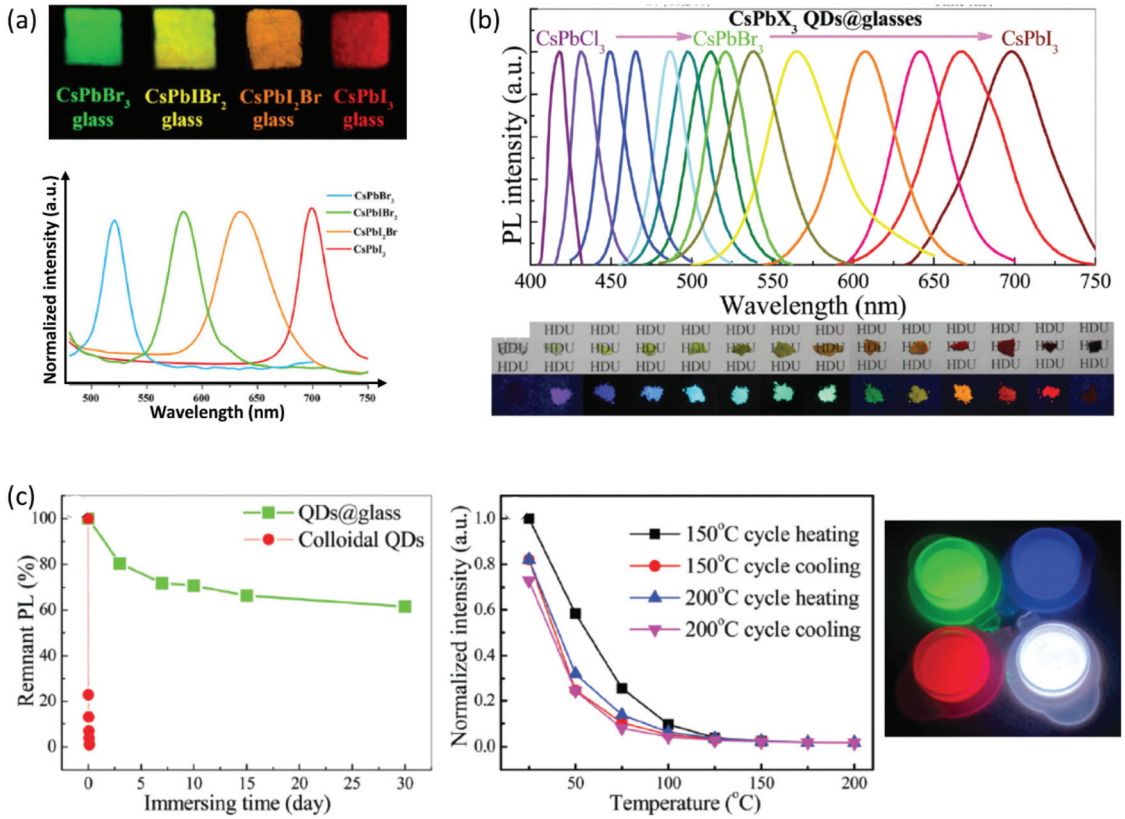

Fig. 4 (a) Optical images of $CsPbX_3$ composite glasses under a 365 nm UV lamp (a has been reproduced from ref. 50 with permission from Elsevier, copyright 2018). (b) Representative PL spectra of $CsPbX_3$ (X = Cl, Cl/Br, Br, Br/I, and I) QD composite borophosphate-based PV-glasses, along with the photographs of the corresponding glass fragments and the perovskite powders under irradiation with a 365 nm UV lamp. (c) Water resistance test of the PL intensity by directly immersing $CsPbBr_3$ QDs composite glasses in aqueous solution, and temperature-dependent emission intensity tests for heating/cooling cycles at 150 and 200 °C. The inset shows luminescence photographs of blue-emitting $CsPbBrCl_2$, green-emitting $CsPbBr_3$, and red-emitting $CsPbBr_{0.5}I_{2.5}$ QD PV-glasses, along with their mixture dispersed in a silicone gel (b and c have been reproduced from ref. 67 with permission from the Royal Society of Chemistry, copyright 2018). All content has been reproduced with permission.

PL water resistance and thermal stability. Upon immersion in water, the pristine perovskite compounds fully degrade within a few hours, whereas the glass encapsulated QDs retain 65% of the initial PL intensity after 30 days (Fig. 4c).[67] In terms of thermal stability, the samples maintain almost 80% of the initial PL intensity after reversible heating and cooling cycles at 150 °C and 200 °C. Following the enhanced stability performance, the authors demonstrated the exploitation of PV-glasses for the development of blue-, green-, and red-emissive light-emitting diode (LED) devices (Fig. 5a and b).[67] Also, a WLED of equally outstanding performance, based on a composite $CsPbBr_3$ QD borosilicate glass, was demonstrated recently by Yang *et al.*[68]

Impressive stability of the emission properties upon humidity exposure and heating was also reported upon using similar composite PNC glass host systems and devices. Zheng *et al.* explored the crystallization mechanism of $CsPbBr_3/Cs_4PbBr_6$ PNCs within borosilicate glasses for the development of a white laser diode of enhanced luminescence efficiency.[60] Five days of exposure to high-temperature (85 °C) and high-humidity (85%) conditions revealed a 20% decrease of the original PL intensity. Meanwhile, the PL intensity was reduced to half following xenon lamp irradiation for the same period. Recently, Zhang *et al.* proceeded one step further, as they demonstrated for the first time the synthesis and simultaneous co-existence of $CsPbCl_3$ and $CsPbI_3$ PNCs within the same borosilicate glass.[61] The combined $CsPbCl_3$:$CsPbI_3$ PNCs exhibited a higher fluorescence emission intensity and higher photoluminescence quantum yield (PLQY) when compared to $CsPbI_3$ PNCs, attributed to a more effective reabsorption of photons (Fig. 5c).[61] Moreover, the $CsPbCl_3$: $CsPbI_3$ PV-glasses displayed remarkable emission stability as the PL intensity remains above 95% after immersion in water for 2 months. As a final part of this study, the authors reported on the development of light-emitting devices upon combining a near infrared emitting composite $CsPbCl_3$: $CsPbI_3$ glass with a 400 nm LED chip, for indoor plant growth (Fig. 5d).[61] Composite borosilicate PV-glasses for the same application have also been reported by Liu *et al.*, upon employing $CsPbBr_1I_2$ and $CsPbCl_2Br_1$ PNC glasses on top of a violet chip.[69]

Another interesting approach for tailoring the emission properties of PV-glasses is by means of chemical

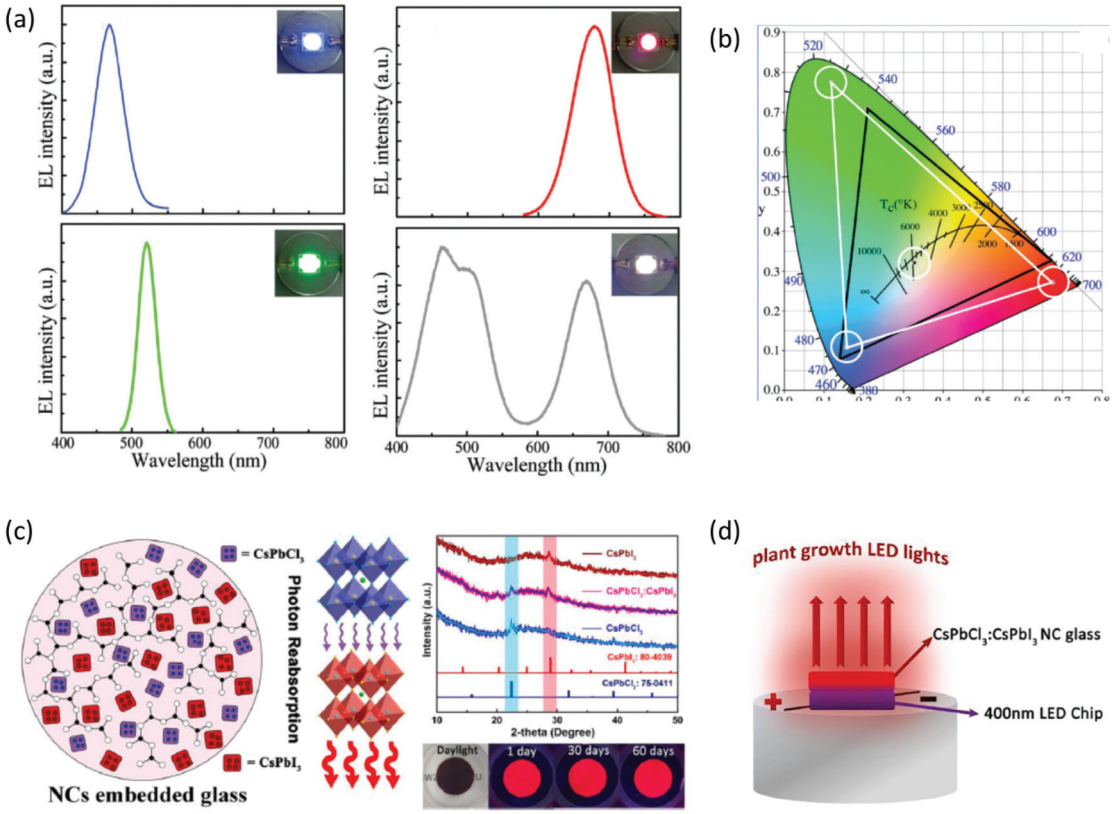

Fig. 5 (a) EL spectra of LED devices captured by coupling blue, green, red glass powders and their mixtures with a UV chip. (b) CIE chromaticity coordinates of the developed LED devices in operation (a and b have been reproduced from ref. 67 with permission from the Royal Society of Chemistry, copyright 2018). (c) Schematic representation of $CsPbCl_3$ and $CsPbI_3$ PNCs co-existence within a borosilicate-based PV-glass, along with the corresponding XRD profiles and photographs of the glass samples taken under UV light after immersion in water for different periods. (d) Schematic illustration of a prototype LED device obtained by coupling the $CsPbCl_3$: $CsPbI_3$ PV-glass with a 400 nm LED chip (c and d have been reproduced from ref. 61 with permission from Elsevier, copyright 2020). All content has been reproduced with permission.

doping.[52,54,55,58,59] For example, Sn-doped $CsPbBr_3$ borosilicate-based composite glasses have been synthesized by typical melt quenching.[52] As depicted in Fig. 6a, in such a system, Sn partly replaces Pb at the B sites of the ABX_3 lattice, for the formation of $CsPb_{1-x}Sn_xBr_3$ QDs. The emission properties of the PV-glasses are strongly related to their Sn/Pb ratios, with a notable blue-shift being observed as x increases (Fig. 6b).[52] The authors attributed the obtained blue-shift to the hybridization of the Pb 6s–B4 4p orbitals. However, the introduction of tin was found to decrease the PLQY of the PNCs due to the reduction of charged exciton formation. Nevertheless, the doped PV-glasses exhibited outstanding PL stability upon humidity exposure for 100 days, as well as, upon heating at 150 °C for 100 h. The application of the Sn-doped composite PV-glass for the development of a WLED was also demonstrated (Fig. 6c).[52] Along similar lines, He *et al.* presented the fabrication of a WLED based on Mn-doped $CsPbBr_xI_{3-x}$ PNCs embedded in glass,[54] whereas Zhao *et al.* demonstrated a WLED based on Cd-doped $CsPbBr_3$ PNCs.[58] Controllable tuning of $CsPbBr_3$ PNC emission properties within a glass was also reported by Zhu *et al.* upon suitable Bi_2O_3 doping for the induction of a spectral blue-shift.[55]

Remarkably, the doping approach opens platforms for additional applications, other than WLEDs. For instance, Zhang *et al.* reported on the fabrication of optical temperature sensing devices of high-sensitivity, based on the doping of glass encapsulated $CsPbI_3$ PNCs with terbium (Fig. 6d).[59] As depicted in Fig. 6d, the synthesized xTb : $CsPbI_3$ PV-glasses exhibit characteristic PL features at 544 nm, 583 nm, 625 nm, and 677 nm. The first three are assigned to the electron transitions of Tb^{3+} ions (Fig. 6e) upon 470 nm laser excitation, whereas the latter is the typical PL signature of the $CsPbI_3$ PNCs. The operation principle of the developed sensor relies on the highly sensitive intensity ratio of the PL relative peaks upon temperature variation.[59] In particular, the features corresponding to the metal element are considerably less sensitive to temperature when compared to the PL band of the $CsPbI_3$ PNCs, which is strongly temperature dependent (Fig. 6d).

Moreover, several groups have investigated the non-linear optical characteristics of composite borosilicate PV-glasses towards ultrafast optical switches and optical limiters. In particular, Jin *et al.* studied for the first time the third-order nonlinear (TONL) optical properties of $CsPbX_3$ (X = Cl/Br, Br)

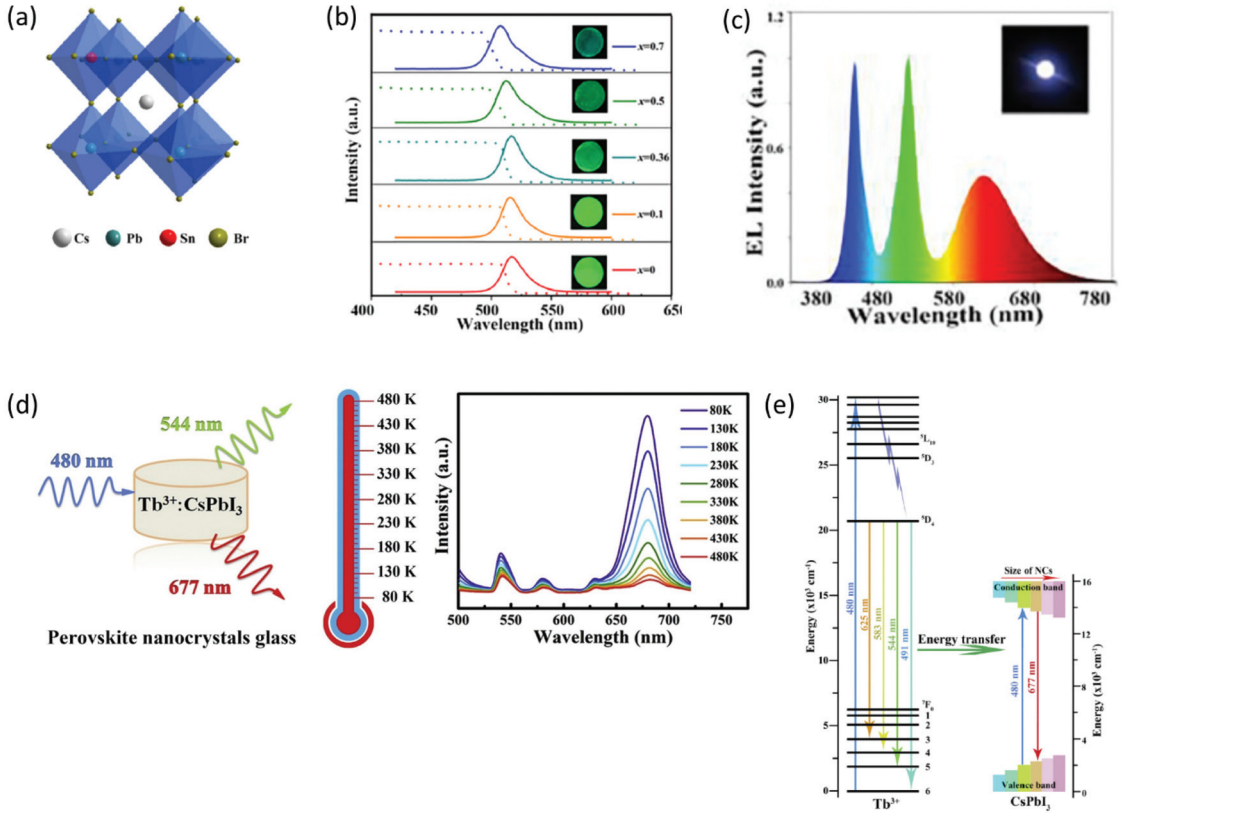

Fig. 6 (a) Crystal structures of Cs-based mixed Pb/Sn perovskites. (b) Absorption and emission spectra of $CsPb_{1-x}Sn_xBr_3$ QDs composite PV-glasses. (c) EL profile of $CsPb_{1-x}Sn_xBr_3$ QDs composite PV-glasses combined with a commercial red phosphor. The inset shows an image of the corresponding WLED device (a–c have been reproduced from ref. 52 with permission from Elsevier, copyright 2019). (d) Schematic animation of the operation principle of a high sensitivity optical temperature sensing device based on a Tb^{3+} : $CsPbI_3$ composite borosilicate PV-glass. (e) Illustration of the corresponding luminescence mechanism and energy bandgaps (d and e have been reproduced from ref. 59 with permission from Elsevier, copyright 2020). All content has been reproduced with permission.

within a borosilicate matrix by means of a non-linear optical imaging technique.[56] All studied composite glasses exhibited strong reverse saturation absorption (RSA), whereas the TONL refractive index relates directly to the composition of the PNCs. Similarly, Xu *et al.* reported on the cross-over from saturated absorption (SA) to (RSA) within a $CsPbBr_3$/borosilicate glass, by either increasing the excitation intensity or the perovskite QD size.[63] The observed RSA was attributed to two-photon absorption that induces strong upconversion luminescence of the embedded QDs. In a rather different manner, Xu *et al.* demonstrated recently the potential application of $CsPbBr_3$-borosilicate glasses as X-ray scintillators.[70] The obtained glasses exhibited a relatively good X-ray response and fast decay when compared to commercially available crystals. Similarly good X-ray scintillating performance was reported for a $CsPb(ClBr)_3$ borate glass by Wang *et al.*,[71] while Niu *et al.* showed the fabrication of a highly stable composite $CsPbBr_3$ tellurite glass nanocomposite scintillator.[72]

Another remarkable feature of composite PV-glasses is the tuning of their emission properties upon incorporation of metal nanoparticles (NPs). Xu *et al.* showed that when silver nanoparticles (AgNPs) are precipitated along with $CsPbBr_3$ QDs inside a borosilicate-based glass, the PL intensity enhances by a factor of five when compared to AgNP free PV-glass.[53] According to the authors, the improved PL is attributed to the accelerated growth of PNCs and the AgNP-induced plasmonic near-field effect. Likewise, Lu *et al.* demonstrated a ten-fold PL efficiency increase upon doping a $CsPbBr_3$ PV-glass with silver,[73] whereas Zhang *et al.* showed a two-fold PL increase in a similar glass system.[74] An additional worth noting feature of composite cesium lead bromide borosilicate glasses was reported recently by Duan *et al.*,[75] as the authors reported on the formation of erasable Cs_4PbBr_6 QDs within the glass matrix. The developed glasses exhibit switchable PL by means of annealing treatments below and above the T_g of the glass.

Inorganic oxide borogermanate and germanate glasses are two more popular types of hosting materials for the incorporation of PNCs.[76,77] Indicatively, Ye *et al.* reported on the growth of $CsPbX_3$ PNCs within borogermanate glasses.[76] PL quantum efficiencies of 80%, 20%, and 20% were reported for $CsPbBr_3$, $CsPb(Cl/Br)_3$, and $CsPb(Br/I)_3$ PNCs, respectively. The samples exhibited remarkable photo and thermal stability, while the fabrication of a WLED was presented upon combin-

ing slices of $CsPbBr_3$ and $CsPb(Br/I)_3$ PV-glasses. The WLED exhibited a luminous efficiency in the range of 50–60 lm W^{-1}, and an external quantum yield of 20–25%.[76] Also, Zhou *et al.* studied the enhanced PL properties of Mn-doped $CsPbCl_3$ and $CsPb(Cl/Br)_3$ PNCs inside a germanate oxide glass.[77] Borotellurite-based glasses offer one more platform for stabilizing PNCs.[78,79] Yuan *et al.* showed the crystallization of $CsPbBr_3$, QDs within a borotellurite glass by means of conventional melting and post-melting annealing treatments, for the development of ultrastable WLEDs.[78] Liu *et al.* proceeded further in exploring the upconversion luminescence of Yb/Ln (Ln = Er, Tm) borotellurite glasses with $CsPbBr_3$ PNCs.[79] Strikingly, apart from the expected green light emission the introduction of lanthanides induced Er^{3+} green, Er^{3+} red, and Tm^{3+} blue upconversion emissions under laser excitation at 980 nm. Upconverting and downshifting emissions were also reported by X. Li *et al.* from $CsPbBr_3$ PNCs triggered by the co-growth of $Tm:NaYbF_4$ crystals within a borogermanate glass.[80] Additionally, Erol *et al.* demonstrated a size-controlled and stable emission of $CsPbBr_3$ QDs embedded in a tellurite matrix upon tailoring the band gap precisely by means of standardized heat treatments.[81]

The last main category of inorganic oxide glasses for hosting PNCs belongs to the phosphate-based family.[82–88] For example, Di *et al.*[83] and Chen *et al.*[84] developed LEDs of excellent stability and performance upon synthesizing $CsPbX_3$ (X = Br, I) within phospho-silicate glasses. Of particular importance is a study by Wang *et al.*, focused on the room temperature synthesis of $CsPbX_3$ (X = Cl, Br, I) QDs on the surface of tin fluorophosphate glasses.[88] Namely, a water-induced surface crystallization mechanism was demonstrated for the first time. According to this hydration mechanism, the water molecules break the P–O–P linkages of the phosphate backbone for the creation of two P–OH chain ends. The obtained depolymerization of the phosphate network results in lowering the crystallization energy of PNCs nearby the glass surface, and consequently in the formation of PNCs.[88] Notably, while the authors report on the thermal stability of the so-formed PNCs, it is very likely that since they are located on the glass surface, and thus, exposed to ambient humidity, their PL features will rapidly degrade with time.[21] Using a similar approach, Li *et al.* impressively reported the feasible formation of $CsPbBr_3$ QDs by means of mechanical and hydration crystallization within a lead containing phosphate glass.[86] Moreover, Ai *et al.*[82] and Chen[85] studied the effect of the employed heating treatment conditions on the PL properties of $CsPbBr_3$ and $CsPbCl_3$ phosphate PV-glasses, respectively. In addition, Li *et al.* presented the synthesis of $CsPbX_3$ (X = Cl, Br, I) PNCs within lead-phosphate glass, towards achieving full visible spectral emission for LED applications.[87] Finally, it is worth mentioning that there are cases where non-inorganic oxide glasses have been employed successfully for the encapsulation of PNCs. Indicatively, Weng *et al.* synthesized α-phase $CsPbI_3$ nanospheres inside a chalcogenide glass matrix.[89] PV-glasses exhibited the typical red emission of the iodine halide, while a temperature size dependence of the perovskite nanospheres was obtained, as the diameter of the spheres was found to increase with temperature.

In summary, the total precursor melting fabrication route appears to be successful in enhancing the PL stability of the encapsulated PNCs, while minimizing lead environmental and health concerns upon keeping the toxic Pb metal trapped within a stable glass matrix. Moreover, the high transparency of inorganic oxide glasses in most of the visible range leaves unaffected the optical and emission properties of the embedded PNCs, towards exploitation for advanced optoelectronic, light emitting, and photonic devices. In contrast to glasses, there are problems when polymer materials are used as hosts, since their non-transparency causes unwanted spectral shifts to the PL profiles of the incorporated PNCs. Despite the great success of the total melting synthesis route, it poses two significant drawbacks. First, it always leads to random positioning of the PNCs throughout the glass matrix (Table 2), which is not facile for the formation of luminescent periodic patterns that are highly important for optoelectronic and photonic applications.[90,91] Secondly, the required high melting temperatures, followed by the elongated post-melting annealing treatments are cost ineffective towards large-scale production and commercialization (Table 2), while accompanied by a significant environmental footprint. Moreover, this route is not feasible for the encapsulation of organic–inorganic halide perovskites due to the volatilization of the organic precursors. It is also worth noting that the post-melting heat treatment during the crystallization process is of critical importance in affecting the quality, as well as the optical and emission properties of the encapsulated PNCs.[62,81,82,85]

2.2.2 Perovskite-glasses by total melting and laser-assisted crystallization. The significance and benefits of employing laser sources for the crystallization of perovskites were reported a few years ago for the growth of organic–inorganic hybrid perovskite films targeting light emitting and energy conversion devices.[92–95] Indeed, it was found that laser-assisted (LA) crystallization results in the formation of more homogeneous perovskite films of better crystalline quality, larger grains, and improved properties. Konidakis *et al.* correlated the superior properties of the LA synthesized films with their advanced exciton dynamics in terms of slower recombination rates and longer free charge carrier diffusion lengths, as probed by means of ultrafast time-resolved transient absorption spectroscopy (TAS).[95,96] Before that, a couple of excellent studies demonstrated the formation of perovskite patterns by means of LA crystallization on the surfaces of various substrates.[90,91] Namely, Arciniegas *et al.* reported on the synthesis of methylammonium lead halide perovskite crystals on typical silicon substrates.[90] By changing the conditions of laser irradiation the authors achieved the controllable growth of perovskite patterns of various shapes (Fig. 7a), towards the development of microplates and wires consisting of methylammonium lead bromide ($MAPbBr_3$) PNCs (Fig. 7b). Along similar lines, Zou *et al.* showed the realization of rewritable photomemory arrays for optical memory applications, based

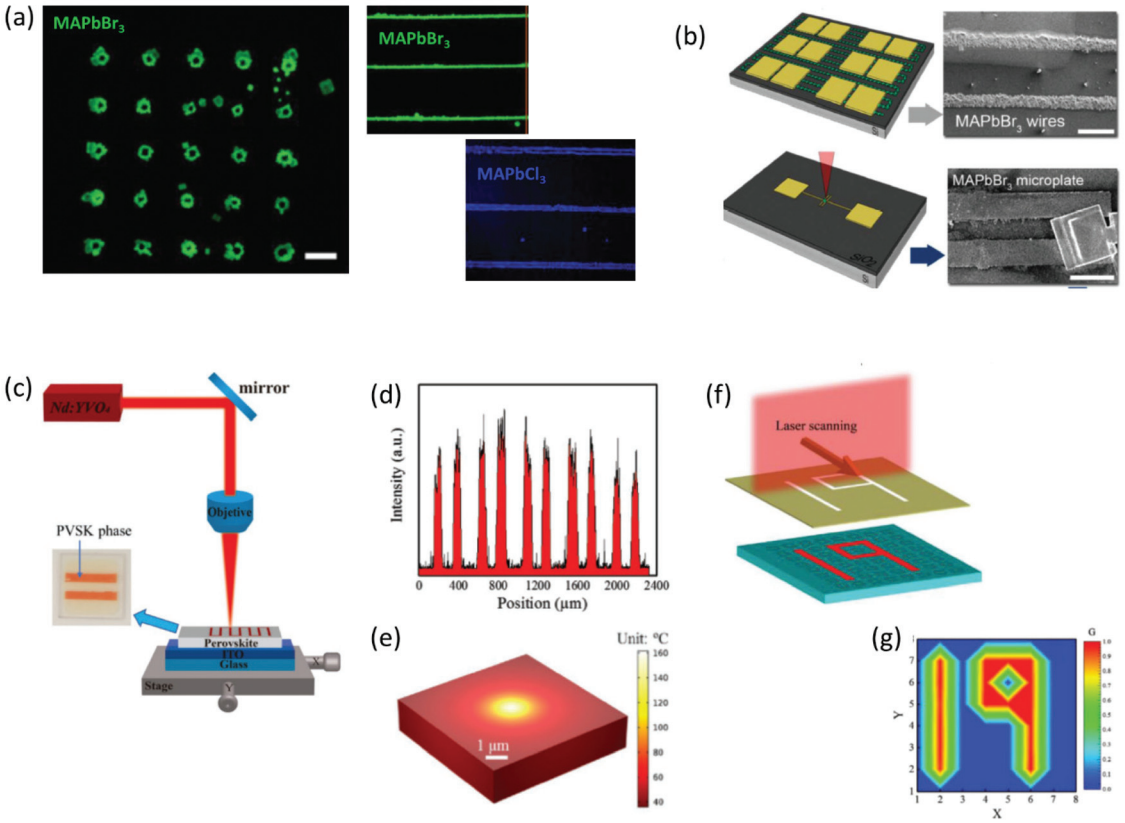

Fig. 7 (a) Fluorescence images of a 5 × 5 $MAPbBr_3$ plate with 150 μm spacing, along with $MAPbBr_3$ and $MAPbCl_3$ wires on silicon substrates captured after laser irradiation. (b) Schematic representation of laser-induced $MAPbBr_3$ microplates and wires for optoelectronic configurations (a and b have been reproduced from ref. 90 with permission from Wiley Online Library, copyright 2017). (c) Experimental setup for the direct laser writing of the perovskite films assisted by the photothermal effect. (d) Line-scan PL intensity of the fluorescence pattern profile. (e) Thermal simulation of heat distribution induced by a laser beam. (f and g) Demonstration of the optical information storage application based on the developed perovskite arrays (c–g have been reproduced from ref. 91 with permission from Wiley Online Library, copyright 2019). All content has been reproduced with permission.

on the reversible phase change of $CsPbIBr_2$ crystals and direct laser writing techniques (Fig. 7c–g).[91] While the results of these studies are of extreme importance and high novelty, the drawbacks of PNC stability and lead toxicity concerns remain, since in both cases the perovskite domains are formed on the substrate surface, and thus possibly degrade due to exposure to ambient air.

Following this, the realization of perovskite crystallization within inorganic oxide glasses by means of ultrafast laser sources was a remarkable breakthrough (Table 2).[97–100] Remarkably, this approach introduced for the first time the opportunity of spatial formation of ultrastable, erasable, and highly luminescent glass-encapsulated periodic patterns.[97,98] Based on this synthesis approach, perovskite and glass precursors are mixed and melted together. Initially the glass is obtained by typical quenching methods. Following this, ultrafast pulsed laser beams that are focused beneath the glass surface initiate the growth of PNCs by means of spatial light-induced heating.[97,98] The optimization of specific laser irradiation parameters and the use of a laser scanning process results in the formation of PNCs patterns inside the glass matrix in a controlled manner. Following this laser induced triggering, for the complete crystallization of the encapsulated PNCs patterns, the composite samples are subjected to typical thermal annealing treatments for several hours within the range of 350–500 °C.

Based on this combined LA-thermal treatment, Huang *et al.* accomplished a three-dimensional patterning of blue emissive $CsPb(Cl/Br)_3$ PNCs inside a borosilicate-based glass with switchable PL.[98] The two-step PNC formation process is schematically depicted in Fig. 8a. At first, in the case of laser irradiation, the crystal lattice can be heated up to thousand degrees in the picosecond time scale *via* the occurring electron–phonon coupling. The high peak power density of femtosecond (fs) lasers renders this possible upon the generation of photoelectrons that transfer their kinetic energy to the crystal lattice.[98] For this purpose, an 800 nm fs laser beam was focused to 500 μm beneath the glass surface, while having a pulse duration of 130 fs and a repetition rate of 1 kHz. A power density of 83×10^2 kW cm^{-2} was used to initiate the formation of crystal nuclei. Meanwhile, the fs laser pulses result in the depolymerization of the borosilicate glass network, which

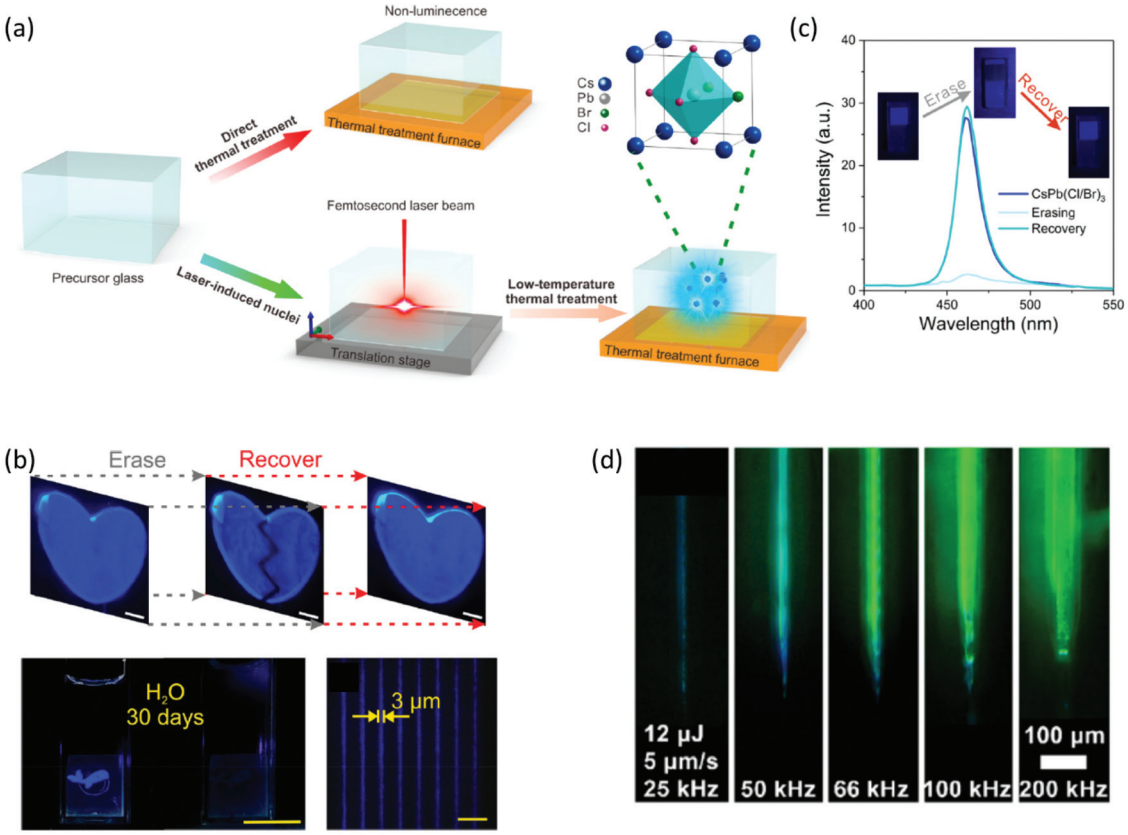

Fig. 8 (a) Schematic animation of the fs laser-induced formation of $CsPb(Cl/Br)_3$ PNCs inside a borosilicate glass. (b) Fluorescence $CsPb(Cl/Br)_3$ patterns showing switchable PL during the erasing/recovery process. (c) Switchable PL profiles and optical images of the $CsPb(Cl/Br)_3$ PV-glasses under UV light excitation recorded during one cycle of the erasing/recovery process (a–c have been reproduced from ref. 98 with permission from American Chemical Society, copyright 2020). (d) Images of written $CsPbBr_3$ lines by means of LA crystallization within a borogermanate glass (d has been reproduced from ref. 99 with permission from American Chemical Society, copyright 2020). All content has been reproduced with permission.

facilitates further atom migration within the matrix. In the second stage, conventional annealing treatment was performed in order to transform the so-formed crystal nuclei into PNCs of good quality. Impressively, the $CsPb(Cl/Br)_3$ PNC formation could be reverted upon further laser irradiation. The erasing of perovskite patterns was carried out upon employing the same fs laser source, while decreasing the power density to 1×10^2 kW cm^{-2}. As a final part of the study, the authors showed the recovery of the PNC patterns upon annealing the samples at 350 °C for 10 min.[98] Thus, a remarkable formation/erasing/recovery cycle of $CsPb(Cl/Br)_3$ PNCs within an inorganic oxide glass is demonstrated (Fig. 8b). Notably, as shown in Fig. 8c the PL profile of the recovered PNCs is in excellent agreement with that of the initially formed crystals. The erasing/recovery part of the cycle was illustrated for up to nine cycles, whereas the PL stability of the perovskite patterns was demonstrated upon immersion in water for 30 days.[98] Such results appear to be very promising for three-dimensional displays, information security protection, and information storage devices (Table 2).

Using a similar approach, Hu *et al.* reported recently on the LA precipitation of $CsPbBr_3$ PNCs inside a borogermanate-based glass for enhancing the performance of a luminescent solar concentrator (LSC).[99] The authors explain that when the embedded PNCs are randomly distributed throughout the glass network, strong self-absorption PL features are induced, and consequently the conversion performance of the device is reduced. In contrast it was shown that when $CsPbBr_3$ parallel lines were synthesized inside the glass by means of fs laser irradiation plus conventional thermal treatment at 400 °C, the quantum efficiency of the solar device architecture enhances significantly.[99] Indicative microscopy images of the PNC lines are presented in Fig. 8d.[99] Likewise, Du *et al.* reported on the formation of $CsPbBr_3$ QDs within borophosphate glasses by heat treatment and ultrafast laser irradiation.[100] A systematic study is performed on the effect of the laser wavelength on the PL properties and stability of PV-glasses.

In summary, the combination of LA procedures along with the typical thermal annealing treatments introduces for the first time a remarkable process of fabricating highly luminescent and stable PNC-based patterns within inorganic oxide glasses. Using this approach, the main disadvantage of total precursor mixing is overcome, as perovskite crystallization occurs in a spatially controllable manner. This is of particular

importance for several optoelectronic and light conversion applications. Nevertheless, it has to be noted that it is a three-step synthesis process including glass melting, ultrafast laser crystallization and subsequent heat treatment.

2.2.3 Perovskite-glasses by post-melting encapsulation. In an entirely different approach the third synthesis route of PV-glasses involves a post-melting incorporation of pre-synthesized PNCs within the glass matrix. In this strategy, the PNCs are prepared separately by means of well-standardized protocols.[64–66,101] In particular, PNCs are embedded by either wet chemistry solvent evaporation or by low-temperature (below 170 °C) annealing treatment of 'soft' glasses. By following the former strategy Shinozaki and Kawano reported on the development of a composite $(C_6H_5C_2H_4NH_3)_2PbBr_4$ borosilicate PV-glass (Fig. 9a).[102] At first, the borosilicate glass substrates were prepared by typical melting-quenching procedures. Then, the substrates were leached with 1 N HNO_3 solution at 363 K for 24 hours, in order to obtain channels and voids throughout the matrix. The as-formed nanoporous glass and appropriate amounts of perovskite precursor powders were mixed in dimethylformamide solvent at 298 K for 1 hour under vacuum. Consequently, the solution penetrates and fills the channels of the nanoporous matrix (Fig. 9a). The inorganic–organic composite PV-glass was obtained upon solvent evaporation at 373 K for 30 min under vacuum, while exhibiting the characteristic PL feature of the $(C_6H_5C_2H_4NH_3)_2PbBr_4$ PNCs.[102] However, it was found that the glass incorporated PNCs exhibited shorter PL lifetimes when compared to the corresponding crystalline samples, due to the quantum confinement effects. In a separate study,[103] the same authors reported on the scintillation properties of the developed organic–inorganic PV-glasses.

Within the same year, Konidakis *et al.* reported for the first time a feasible method for the development of PV-glasses by means of PNC post-melting encapsulation and low-temperature annealing treatment (Table 2).[104] Based on this approach, pre-synthesized $CsPbBr_3$ PNCs were encapsulated within a 'soft' silver metaphosphate ($AgPO_3$) glass. Notably, the PNCs

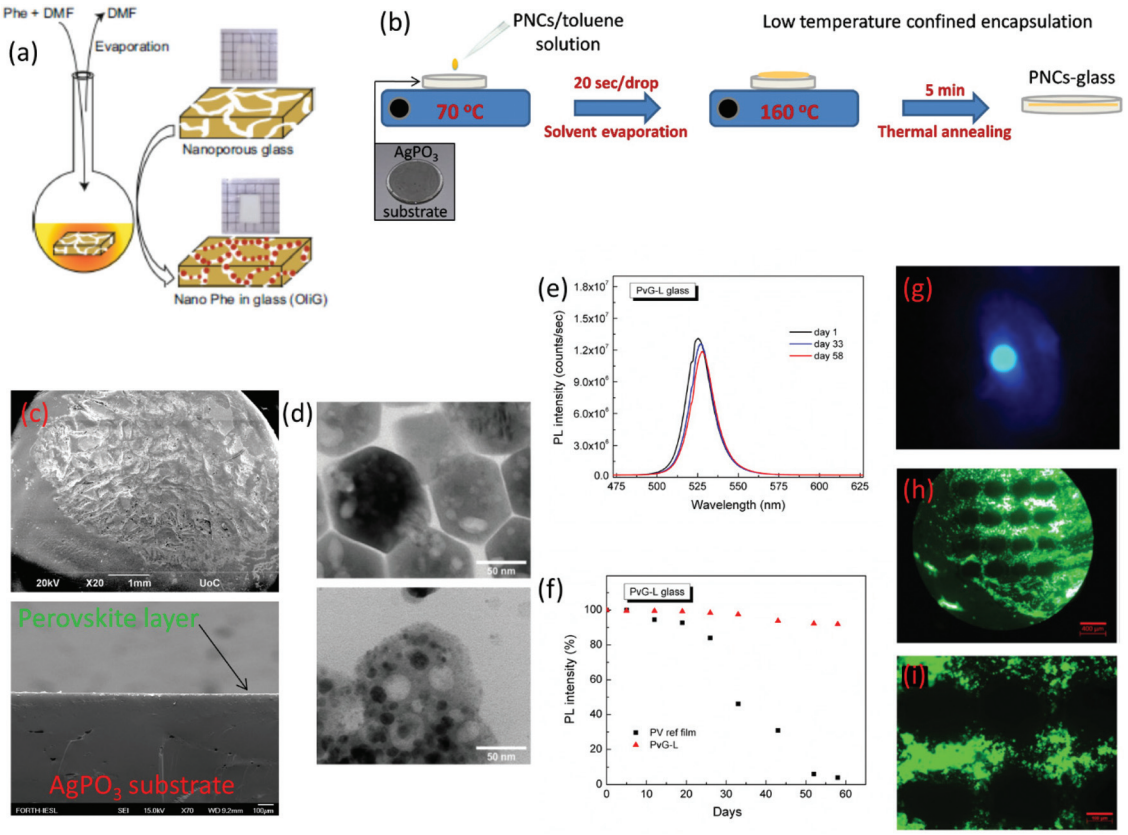

Fig. 9 (a) Process of filling the porous of a borosilicate glass with organic–inorganic $(C_6H_5C_2H_4NH_3)_2PbBr_4$ PNCs by means of a solvent evaporation process (a has been reproduced from ref. 102 with permission from Nature, copyright 2020). (b) Schematic demonstration of the post glass melting encapsulation process of PNCs within glasses. (c) Scanning electron microscopy (SEM) images of the PV-glass surface and cross-section after vitrification of the perovskite layer. (d) Transmission electron microscopy (TEM) profiles of the $CsPbBr_3$ PNCs before (upper figure) and after (lower figure) glass encapsulation. (e) Indicative PL spectra of the composite $CsPbBr_3$-phosphate PV-glass over a period of two months. (f) Percentage of the maintained PL intensity *versus* days of exposure to ambient air. (g) Photograph of $CsPbBr_3$-phosphate PV-glass green luminescence with a visible scattering of the blue excitation laser. (h and i) Fluorescence photos of $CsPbBr_3$ microdotted optical textures encapsulated within silver phosphate glass (b–i have been reproduced from ref. 104 with permission from the Royal Society of Chemistry, copyright 2020). All content has been reproduced with permission.

were derived from a facile room-temperature co-precipitation method, whereas the selection of the $AgPO_3$ glass was prompted by its low T_g of 192 °C, and high transparency in most of the visible range.[105] The fabrication route is depicted schematically in Fig. 9b. Namely, several drops of $CsPbBr_3$/toluene solution (50 mg ml^{-1}) were added to the $AgPO_3$ glass substrate heated at 70 °C. This temperature facilitates the gentle vaporization of toluene for the formation of the $CsPbBr_3$ precipitate on the entire glass surface. Then the temperature was increased to 160 °C for 5 min, *i.e.* 32 °C below the T_g of $AgPO_3$ glass.[104] At this temperature the $AgPO_3$ glass gains viscosity and enables the controllable incorporation of a PNC layer beneath the surface. After the perovskite layer immersion was complete, the glass was instantly removed from the heating plate, and allowed to cool down at room temperature. Fig. 9c shows the indicative scanning electron microscopy (SEM) photos of the surface after PNC vitrification, whereas Fig. 9d presents the corresponding transmission electron microscopy (TEM) profiles of the $CsPbBr_3$ PNCs before and after encapsulation. Inspection of TEM photos revealed that the embedded $CsPbBr_3$ crystals almost retain their shape and characteristics, suggesting that the low-temperature encapsulation protocol had no effect on their nature. Moreover, a thorough Raman analysis revealed that the incorporation of PNCs has no effect on the connectivity of the phosphate glass network.[104]

The developed phosphate-based PV-glasses exhibited the distinct PL profile of the $CsPbBr_3$ PNCs while showing remarkable PL stability. Fig. 9e depicts the indicative PL spectra of the $CsPbBr_3$–$AgPO_3$ glass over a period of two months, while Fig. 9f shows how the PL intensity varies with time. Fig. 9g presents a photo of the green photoluminescence of the PV-glass, along with some scattering of the blue excitation laser. Impressively, the composite glass retains around 97% of the initial intensity during the first month, while after two months it exhibits minimal losses of around 8% (Fig. 9f).[104] Notably, the corresponding losses of the air-exposed $CsPbBr_3$ PNCs are 55% and 96%, respectively. Thus, as in all previously reported cases (Table 2), the post-glass melting encapsulation protocol offers equally good luminescence stability. In addition, as a final part of the study, the authors demonstrated the formation of ultrastable and highly luminescent perovskite periodic micropatterns within the glass matrix by means of a continuous wave (cw) laser irradiation process.[104] Fig. 9h and i show the selective fluorescence photographs of micro-dotted optical textures under UV light irradiation, after performing laser patterning with a cw 455 nm laser. The distance between the dots is readily defined by the horizontal and vertical separation steps, whereas the diameter of the dots is controlled by the employed spot size of the cw laser. Also, the authors compared the PL profiles of the PV-glass prior to laser processing and after the micropattern formation, and found only negligible differences. Therefore, it was concluded that the laser processing procedure was not affecting the luminescence properties of the glass embedded PNCs.

In conclusion, post-melting incorporation of PNCs within glasses is possible in two ways. The solvent evaporation method allows the filling of porous glasses with PNCs. The big advantage of this procedure is that it allows the inclusion of both organic–inorganic and all-inorganic perovskite crystals within oxide glasses. However the PV-glasses obtained using this route pose the limitation of reduced transparency due to the presence of the nanoporous channels. It has to be noticed also that in this case the PNCs are not entirely mixed within the glass network, but rather differently they exist as a separate phase within the glass host. On the other hand, the low-temperature annealing method is an outstanding protocol for the confined positioning of all types of inorganic PNCs within glasses of low T_g values. Meanwhile it creates a platform for the feasible formation of luminescent micropatterns by means of widely available, compact, low-cost, cw laser sources, while being extremely fast and efficient. Based on this, it is expected to pave the way for the development of advanced composite perovskite–glass architectures for various photonic and optoelectronic applications. Nevertheless, it can only be applied for soft glasses of low T_gs, while to this date the erase/recovery feature for reversible PL emission has not been investigated.

2.3 Two-dimensional (2D) material composite glasses

Since the accomplishment of graphene isolation in 2004, 2D materials have gained a lot of attention due to their unique optical and electrical properties. In an effort to explore the potential of this type of material and also to protect them from corrosion, research has been done to incorporate 2D materials in different systems, such as transparent thermoplastic glasses (TTGs) and inorganic oxide glass matrices.

TTGs, such as polymethylmethacrylate (PMMA), have been used for embedding transition metal disulfides (TMDs) in order to investigate their nonlinear optical (NLO) properties. The choice of PMMA as a host is made due to its ease to melt, its advantageous mechanical properties, low cost and most importantly its stable optical properties. Tao *et al.* reported on the successful homogeneous incorporation of MoS_2 nanosheets into PMMA and the non-linear optical (NLO) properties of the composite glass were investigated by a nanosecond pulsed Nd:YAG laser.[106] The results of this work showed good NLO properties for both 532 and 1064 nm, attributed to the low, NLO onset threshold F_{ON}, low optical limiting threshold F_{OL}, and low optical limiting differential transmittance T_C, while exhibiting a high two-phonon absorption coefficient β at both wavelengths. Regarding the same MoS_2/PMMA composite architecture, Liang *et al.* investigated the NLO properties using an 800 nm ultrafast laser.[107] The authors of this study concluded that as the concentration of MoS_2 increases in the PMMA there is an increase in the optical limiting response. Another work by Wei *et al.* is based on the synthesis and optical characterization of WS_2/PMMA by a fs laser at 800 nm.[108] Driven by similar observations to the two previously reported systems the studied composite 2D-materials/PMMA architectures could be employed in optical limiter devices and applications.

Inorganic oxide glasses, in contrast to PMMA polymer-based hosts, provide advantages for the incorporation of 2D

materials aimed to be used in optoelectronics. This is because they usually exhibit higher glass transition temperatures (T_g). Moreover, PMMA is almost non-transparent in the deep UV spectral region, a characteristic that lays down limitations to potential optoelectronic and photonic applications. For instance, several types of glasses have been used for the incorporation of graphene oxide (GO) based 2D-materials (Table 3). Notably, GO is widely used because aside from its linear optical properties, its 2D nature merged with the tunable optical bandgap lead to interesting nonlinear optical features, such as nonlinear optical absorption. This change in absorption with light intensity can appear as reverse saturable absorption (RSA) which is useful for optical limiters, though it depends on the excitation wavelength, as well as on the bandgap of the employed GO compound. Based on the above results, there is a continuous scientific challenge in exploring new synthetic methods for the incorporation of GO-based materials into solid hosts.

Indicatively, Tao *et al.* reported a novel synthesis of silica gel glass with homogeneous dispersion of GO.[109] At first, GO nanosheets are functionalized with 3-aminopropyltriethoxysilane (APTES), then the GO-APTES are introduced to the silica matrix through a sol–gel process. Following this, they are hydrolyzed and finally the GO sheets are covalently bonded to the silica matrix. Remarkably, the investigation of NLO properties of the developed composite silica gel glass and the typical GO aqueous solution revealed that the NLO properties of the former were enhanced. Along similar lines, Zheng *et al.* reported on the successful incorporation of GO nanosheets (GONS) and nanoribbons (GONR) in modified silicate (Ormosil) gel glass by the sol–gel synthesis method.[110] Fig. 10a presents the photos of the developed GO/glasses gel glasses, whereas Fig. 10b depicts the open-aperture Z-scan experimental setup for the normalized transmittance results shown in Fig. 10c for an incident energy of 200 μJ. Inspection of Fig. 10c reveals symmetric curves before and after passing through the focus with a deep valley observed as the sample passes through the focal point, *i.e.* indicative of a typical NLO response.[110] It was also shown that the developed composite glasses were sustainable to continuous laser pulses with an incident energy of 800 μJ. Such findings demonstrate that GO-based/glass composite configurations offer a potential platform for optical limiter devices and applications.

On the other hand, molybdenum disulfide (MoS_2) has also gained a lot of attention not only for its NLO properties but also for its photoluminescence (PL) features. By coupling 2D MoS_2 with nanomaterials it is possible to manipulate its PL, although there isn't a great amount of research regarding few-layer MoS_2. A recent study by Sarkar *et al.*[111] provides a novel synthetic route for the incorporation of MoS_2 flakes inside a silver metaphosphate ($AgPO_3$) glass (Fig. 10d). The main objective of this study was to obtain a facile method for tailoring and enhancing the exciton emission of this particular transition metal dichalcogenide (TMD). This aim was achieved by means of silver plasmon resonance effects that occur within the silver-rich phosphate glass. In particular, MoS_2 flakes were incorporated within the glass *via* a post-glass melting encapsulation protocol depicted in Fig. 10d.[111] Several drops of an as-prepared MoS_2/isopropanol solution were dropcast on the glass substrate. Following this, the glass was heated to 170 °C, gained viscosity, and allowed the immersion of the 2D crystals beneath the surface, *i.e.* in a similar manner to that described in section 2.2.3 for PV-glasses. The obtained composite $MoS_2:AgPO_3$ nanoheterojunction architectures exhibited remarkable PL features as recorded by micro-PL spectroscopy. Fig. 10e presents the steady-state room temperature PL spectra of pristine $AgPO_3$ glass, of MoS_2 on a typical silicon substrate (Si/MoS_2), and of the composite $AgPO_3:MoS_2$ glass, upon using an excitation energy of 2.28 eV (543 nm). It is notable that the MoS_2 PL profile changes dramatically upon incorporation within $AgPO_3$ glass. In fact, the $AgPO_3:MoS_2$ PL spectrum exhibited two well-defined emission peaks at 1.89 and 2.05 eV, corresponding to A- and B-excitonic transitions, respectively.[111] Meanwhile, an impressive 6-fold enhancement is observed for the B-exciton peak intensity. The authors attributed the observed enhancement to the dipole–dipole interaction *via* exciton–plasmon coupling induced by the presence of silver nanoparticles (AgNPs) throughout the glass. Notably, the described encapsulation method can be applied for the incorporation of any two-dimensional (2D) material within inorganic oxide glass, providing that the 2D material can sustain the heating near the glass transition temperature of the glass.

Table 3 Summary of two-dimensional (2D) material composite glasses, along with brief details of the fabrication protocols, and key features of the optical properties

Study-year	Composite glass system	Synthesis protocol	Melting and annealing treatment	Key features and potential applications
2D materials composite glasses				
Tao *et al.*, 2014[106]	MoS_2-PMMA	Mixed and heated	75 °C, 30 h	NLO features/optical limiter
Liang *et al.*, 2019[107]	MoS_2-PMMA	Mixed and heated	75 °C, 30 h	NLO features/solid-state optical limiter
Wei *et al.*, 2016[108]	WS_2-PMMA	Mixed and heated	75 °C, 30 h	NLO features/optical limiter
Tao *et al.*, 2013[109]	Graphene oxide–silica gel glass	Chemical process	—	NLO features/optical limiter
Zheng *et al.*, 2013[110]	Graphene oxide–silica gel glass	Sol–gel method	—	NLO features/optical limiter
Sarkar *et al.*, 2020[111]	MoS_2–$AgPO_3$	Post-glass melting encapsulation	M: 450 °C A: 170 °C	Enhanced RT B-exciton emission/nanophotonic, valleytronic, and optoelectronic devices

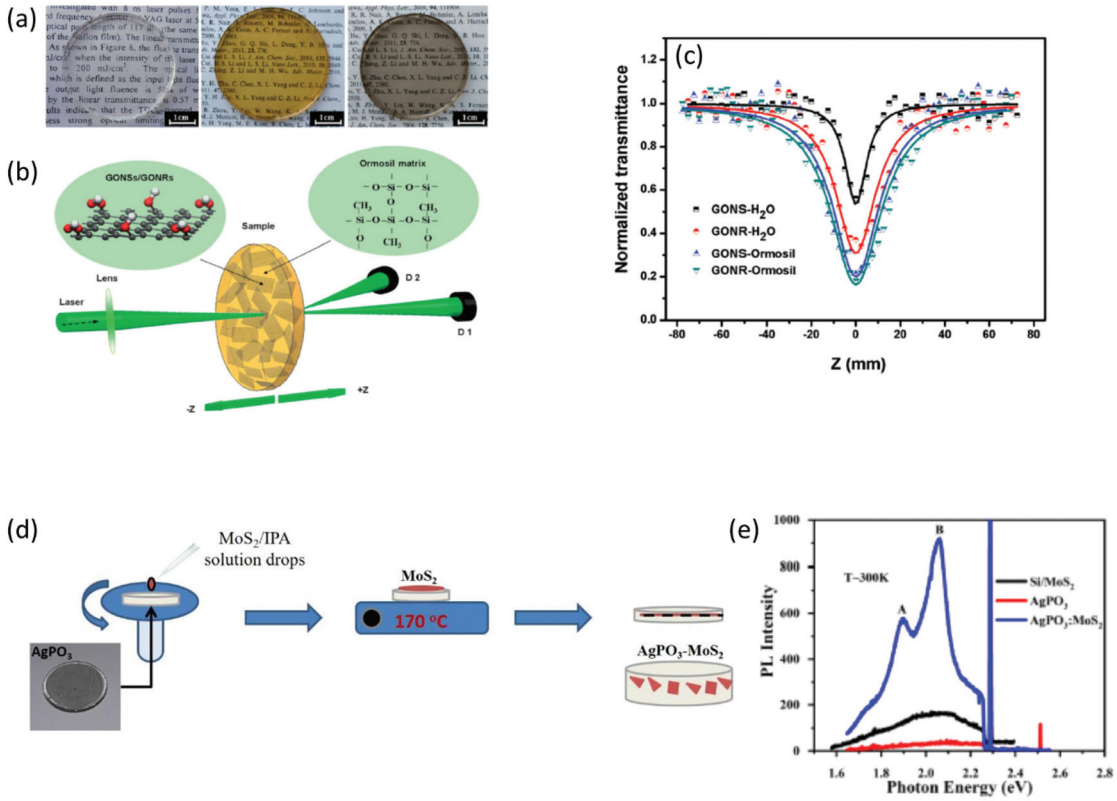

Fig. 10 (a) Photographs of the undoped silicate glass, and the composite GONS/silicate and GONR/silicate gel glasses. (b) Schematic representation of the open-aperture Z-scan experimental setup. (c) Open-aperture Z-scan normalized transmittance at 200 μJ (a–c have been reproduced from ref. 110 with permission from the Royal Society of Chemistry, copyright 2013). (d) Post-glass melting encapsulation protocol of MoS_2 flakes in glass. (e) PL spectra of $AgPO_3$ glass, Si/MoS_2, and composite $AgPO_3$: MoS_2 glass (d and e have been reproduced from ref. 111 with permission from Nature, copyright 2020). All content has been reproduced with permission.

The reported fabrication protocol might be of particular importance for the large scale production of inexpensive nanophotonic, valleytronic, and optoelectronic devices with tunable B-excitonic emissions.

3. General remarks and conclusions

The purpose of this review is to demonstrate the potential advantages and possibilities when nanocrystalline materials and metallic nanoparticles are incorporated within glass matrices. More importantly, it provides an overview of the available fabrication routes, while assessing their advantages and drawbacks with respect to the properties and potential applications.

Scientific interest for perovskite glasses (PV-glasses) emerged exponentially during the last three years or so, in an attempt to stabilize the perovskite crystals while reducing the risks of lead contamination. Due to their transparency in a broad spectral range, inorganic oxide glasses present the most attractive host platform. As discussed thoroughly, there are three main fabrication routes for the development of advanced composite PV-glasses. These are (i) the total mixing-melting of glass and perovskite precursors, (ii) the total mixing-melting with the assistance of ultrafast laser sources, and (iii) the post-glass melting encapsulation of previously prepared PNCs. All of them resolve the main scientific challenge of improving the luminescence stability of the embedded PNCs. The latter two also provide the additional and significant advantage of allowing the formation of ultrastable and highly luminescent domains and periodic micropatterns within the stable environment of the glass network. Based on these important scientific advancements, in the near future composite PV-glasses are expected to play an important role in various state-of-the-art photonic and optoelectronic applications, such as light emitting platforms, high-capacity optical memory components, information encryption, 3D artworks, plant growth devices, scintillators, optical temperature sensing, and photodetectors, among others.

Rather differently, in the cases of 2D materials the glass encapsulation concept was prompted by other reasons. Nowadays the enormous potential of 2D materials in next-generation photonic applications has been well recognized. Nevertheless, continuous scientific efforts are dedicated to the enhancement of 2D material emission properties. As presented by a series of recent studies, the incorporation of 2D materials within polymer-glasses and glasses offers a nano-architecture for further tailoring their excitonic features while inducing nonlinear optical characteristics. Based on this, the encapsulation approach appears promising towards boosting

the nanophotonic, valleytronic, and optoelectronic future applications of composite 2D material/glass configurations.

In the case of metal NPs, their incorporation within glasses is mainly triggered by the enhancement of the emission properties and the introduction of various functional features. In this view several composite metal NPs glass systems have been investigated over the years. Herein we considered a wide selection of scientific studies in order to provide information on the synthesis of the composite systems while demonstrating how the induced plasmon resonance coupling interactions are exploited towards advancing the optical properties. For instance there are several examples where the incorporation of metal NPs is accompanied by the introduction of important second and third nonlinear optical features that can be readily exploited towards advanced photonic applications. Along the same lines, the encapsulation of NPs inside glasses offers an ideal route towards the realization of advanced optical modulator devices with tunable light emission and lasing features. On the other hand, the introduction of NPs within glasses may also induce changes in the surface wettability properties targeting self-cleaning and fluid transport applications. In the same manner, the incorporation of metal NPs within bioresorbable glasses could provide great potential for improving surface hygiene through the development of advanced antivirus coatings. In addition, the presence of metal NPs inside inorganic oxide glasses could pave the way for the design of modern antireflecting coatings for camouflage operations, and military protection against aging and ballistic threats. Finally, important advantages may arise in the field of photocatalysis for the production and storage of next-generation biofuels, upon the employment of glass reactors that are capable of directing light at the atomic level by means of NP scattering effects within the composite glass surroundings.

Conflicts of interest

There are no conflicts to declare.

Acknowledgements

This work was partially supported by the SmartMat project, "Laser-assisted development of composite thermochromic materials for energy smart and safe buildings", ΕΣΠΑ2014-2020, RIS3Crete, G.A. KPHP1-0032623.

References

1 K. Hughes, *Physics of Electrolytes*, Academic Press, Cambridge, 1972, Vol. 1, p. 10.
2 A. R. West, *Solid State Chemistry and its Applications*, Wiley-Blackwell, Hoboken, 1984, p. 18.
3 I. Konidakis, PhD Thesis, University of Aberdeen, 2006.
4 B. E. Warren and J. Biscob, *J. Am. Ceram. Soc.*, 1938, **21**, 259.
5 W. J. Stark, P. R. Stoessel, W. Wohllebenb and A. Hafnerc, *Chem. Soc. Rev.*, 2015, **44**, 5793.
6 S. Mukherji, S. Bharti, G. Shukla and S. Mukherji, *Phys. Sci. Rev.*, 2019, **4**, 20170082.
7 A. Kojima, K. Teshima, Y. Shirai and T. Miyasaka, *J. Am. Chem. Soc.*, 2009, **131**, 6050.
8 H. J. Snaith, *J. Phys. Chem. Lett.*, 2013, **4**, 3623.
9 P. Gao, M. Grätzel and M. K. Nazeeruddin, *Energy Environ. Sci.*, 2014, **7**, 2448.
10 S. D. Stranks and H. J. Snaith, *Nat. Nanotechnol.*, 2015, **10**, 391.
11 M. I. Saidaminov, J. Almutlaq, S. Sarmah, I. Dursun, A. A. Zhumekenov, R. Begum, J. Pan, N. Cho, O. F. Mohammed and O. M. Bakr, *ACS Energy Lett.*, 2016, **1**, 840.
12 E. Y. Tiguntseva, G. P. Zograf, F. E. Komissarenko, D. A. Zuev, A. A. Zakhidov, S. V. Makarov and Y. S. Kivshar, *Nano Lett.*, 2018, **18**, 1185.
13 G. Xing, N. Mathews, S. S. Lim, N. Yantara, X. Liu, D. Sabba, M. Grätzel, S. Mhaisalkar and T. C. Sum, *Nat. Mater.*, 2014, **13**, 476.
14 Y. Fu, H. Zhu, C. C. Stoumpos, Q. Ding, J. Wang, M. G. Kanatzidis, X. Zhu and S. Jin, *ACS Nano*, 2016, **10**, 7963.
15 L. Dou, Y. M. Yang, J. You, Z. Hong, W. H. Chang, G. Li and Y. Yang, *Nat. Commun.*, 2014, **5**, 5404.
16 Y. Fang, Q. Dong, Y. Shao, Y. Yuan and J. Huang, *Nat. Photonics*, 2015, **9**, 679.
17 M. Ahmadi, T. Wu and B. Hu, *Adv. Mater.*, 2017, **29**, 1605242.
18 H. C. Wang, S. Y. Lin, A. C. Tang, B. P. Singh, H. C. Tong, C. Y. Chen, Y. C. Lee, T. L. Tsai and R. S. Liu, *Angew. Chem., Int. Ed.*, 2016, **55**, 7924.
19 M. Grätzel, *Nat. Mater.*, 2014, **13**, 838.
20 B. Hailegnaw, S. Kirmayer, E. Edri, G. Hodes and D. Cahen, *J. Phys. Chem. Lett.*, 2015, **6**, 1543.
21 P. Docampo and T. Bein, *Acc. Chem. Res.*, 2016, **49**, 339.
22 K. Uchida, S. Kaneko, S. Omi, C. Hata, H. Tanji, Y. Asahara, A. J. Ikushima, T. Tokizaki and A. Nakamura, *J. Opt. Soc. Am.*, 1994, **11**, 7.
23 H. Hofmeister, S. Thiel, M. Dubiel and E. Schurig, *Appl. Phys. Lett.*, 1997, **70**, 1694.
24 A. Simo, J. Polte, N. Pfänder, U. Vainio, F. Emmerlin and K. Rademann, *J. Am. Chem. Soc.*, 2012, **134**, 18824.
25 G. Venkateswara Rao and H. D. Shashikala, *J. Alloys Compd.*, 2015, **622**, 108.
26 X.-C. Yang, Z. W. Dong, H. X. Liu, J. X. Xu and S. X. Qian, *Chem. Phys. Lett.*, 2009, **475**, 256.
27 A. Pan, Z. Yang, H. Zheng, F. Liu, Y. Zhu, X. Su and Z. Ding, *Appl. Surf. Sci.*, 2003, **205**, 323.
28 G. Venkateswara Rao and H. D. Shashikala, *J. Non-Cryst. Solids*, 2014, **402**, 204.
29 T. Som and B. Karmakar, *J. Opt. Soc. Am. B*, 2009, **26**, 12.
30 I. Soltani, S. Hraiech, K. Horchani-Naifer, J. Massera, L. Petit and M. Férid, *J. Non-Cryst. Solids*, 2016, **438**, 67.

31 I. Soltani, S. Hraiech, K. Horchani-Naifer, H. Elhouichet, B. Gelloz and M. Férid, *J. Alloys Compd.*, 2016, **686**, 556.
32 I. Soltani, S. Hraiech, K. Horchani-Naifer and M. Férid, *Opt. Mater.*, 2018, **77**, 161.
33 H. Nurhafizah, M. S. Rohani and S. K. Ghoshal, *J. Non-Cryst. Solids*, 2016, **455**, 62.
34 M. Haouari, F. Ben Slimen, A. Maaoui and N. Gaumer, *J. Alloys Compd.*, 2018, **743**, 586.
35 J. Zmojda, P. Miluski and M. Kochanowicz, *Appl. Sci.*, 2018, **8**, 790.
36 R. Vijayakumar and K. Marimuthu, *J. Alloys Compd.*, 2016, **665**, 294.
37 C. Hua, L. Shen, E. Y. B. Pun, D. Li and H. Lin, *Opt. Mater.*, 2018, **78**, 72.
38 G. Lakshminarayana and J. Qiu, *J. Alloys Compd.*, 2009, **478**, 630.
39 T. M. Machado and M. A. P. Silva, *Mater. Chem. Phys.*, 2020, **244**, 122731.
40 M. K. Halimah, A. M. Hamza, F. D. Muhammad, K. T. Chan, S. A. Umar, I. Umaru and I. G. Geidam, *Mater. Chem. Phys.*, 2019, **236**, 121795.
41 T. M. Machado, R. F. Falci, I. L. Silva, V. Anjos, M. J. V. Bell and M. A. P. Silva, *Mater. Chem. Phys.*, 2019, **224**, 73.
42 A. Podlipensky, A. Abdolvand, G. Seifert, H. Graener, O. Deparis and P. G. Kazansky, *J. Phys. Chem. B*, 2004, **108**, 46.
43 J. Sasai and K. Hirao, *J. Appl. Phys.*, 2001, **89**, 4548.
44 S. Singla, V. G. Achanta, O. P. Pandey and G. Sharma, *Ceram. Int.*, 2020, **46**, 9907.
45 I. Konidakis, S. Psilodimitrakopoulos, K. Kosma, A. Lemonis and E. Stratakis, *Opt. Mater.*, 2018, **75**, 796.
46 I. Konidakis, G. Zito and S. Pissadakis, *Opt. Lett.*, 2012, **37**, 2499.
47 I. Konidakis and S. Pissadakis, *Materials*, 2014, **7**, 5735.
48 P. Li, C. Hu, L. Zhou, J. Jiang, Y. Cheng, M. He, X. Liang and W. Xiang, *Mater. Lett.*, 2017, **209**, 483.
49 P. Li, C. Hu, L. Zhou, J. Jiang, Y. Cheng, M. He, X. Liang and W. Xiang, *Mater. Res. Bull.*, 2018, **105**, 63.
50 S. Liu, M. He, X. Di, P. Li, W. Xiang and X. Liang, *Ceram. Int.*, 2018, **44**, 4496.
51 S. Liu, Y. Luo, M. He, X. Liang and W. Xiang, *J. Eur. Ceram. Soc.*, 2018, **38**, 1998.
52 S. Liu, G. Shao, L. Ding, J. Liu, W. Xiang and X. Liang, *Chem. Eng. J.*, 2019, **361**, 937.
53 Z. Xu, X. Liu, J. Qiu and C. Cheng, *Opt. Lett.*, 2019, **44**, 5626.
54 M. He, L. Ding, S. Liu, G. Shao, Z. Zhang, X. Liang and W. Xiang, *J. Alloys Compd.*, 2019, **780**, 318.
55 Y. Zhu, B. Yang, Q. Lu, Y. Li, M. Shi and J. Zou, *ECS J. Solid State Sci. Technol.*, 2020, **9**, 126003.
56 M. Jin, X. Liang, H. Zhang, J. Liu, G. Shao, W. Xiang and Y. Song, *J. Eur. Ceram. Soc.*, 2020, **40**, 4140.
57 B. Yang, F. Zheng, S. Mei, Z. Chen, Y. Xie, H. Dai, X. Wei, W. Zhang, F. Xie, J. Ju, Y. Chu, J. Zou and R. Guo, *Appl. Surf. Sci.*, 2020, **512**, 145655.
58 Y. Zhao, C. Shen, L. Ding, J. Liu, W. Xiang and X. Liang, *Opt. Mater.*, 2020, **107**, 110046.
59 Y. Zhang, J. Liu, H. Zhang, Q. He, X. Liang and W. Xiang, *J. Eur. Ceram. Soc.*, 2020, **40**, 6023.
60 F. Zheng, B. Yang, P. Cao, X. Qian and J. Zou, *J. Alloys Compd.*, 2020, **818**, 153307.
61 Z. Zhang, L. Shen, Y. Zhao, Y. Zhang, H. Yang, W. Xiang, X. Liang, G. Chen and H. Yu, *Chem. Eng. J.*, 2020, **385**, 123415.
62 X. Liu, E. Mei, Z. Liu, J. Du, X. Liang and W. Xiang, *ACS Photonics*, 2021, **8**, 887.
63 Z. Xu, T. Chen, D. Zhang, G. Zheng, J. Wu, J. Yan, X. Liu and J. Qiu, *J. Eur. Ceram. Soc.*, 2021, **41**, 729.
64 L. Protesescu, S. Yakunin, M. I. Bodnarchuk, F. Krieg, R. Caputo, C. H. Hendon, R. X. Yang, A. Walsh and M. V. Kovalenko, *Nano Lett.*, 2015, **15**, 3692.
65 Q. A. Akkerman, S. Park, E. Radicchi, F. Nunzi, E. Mosconi, F. D. Angelis, R. Brescia, P. Rastogi, M. Prato and L. Manna, *Nano Lett.*, 2017, **17**, 1924.
66 F. Palazon, C. Urso, L. D. Trizio, Q. Akkerman, S. Marras, F. Locardi, I. Nelli, M. Ferretti, M. Prato and L. Manna, *ACS Energy Lett.*, 2017, **2**, 2445.
67 D. Chen, S. Yuan, J. Chen, J. Zhong and X. Xu, *J. Mater. Chem. C*, 2018, **6**, 12864.
68 Z. Yang, H. Zhang, Z. Fang, J. Yi, P. Song, X. Yu, D. Zhou, J. Qiu and X. Xu, *Chem. Eng. J.*, 2022, **427**, 131379.
69 J. Liu, L. Shen, Y. Chen, Y. Zhao, Y. Zhang, M. Jin, H. Yang, Y. Zhang, W. Xiang and X. Liang, *J. Mater. Chem. C*, 2019, **7**, 13606.
70 Y. Xu, X. Zhao, M. Xia and X. Zhang, *J. Mater. Chem. C*, 2021, **9**, 5452.
71 C. Wang, H. Lin, Z. Zhang, Z. Qiu, H. Yang, Y. Cheng, J. Xu, X. Xiang, L. Zhang and Y. Wang, *J. Eur. Ceram. Soc.*, 2020, **40**, 2234.
72 L. Niu, S. Wang, Z. Sui, Y. Song, L. Zhao, L. Liu, J. Ren and J. Zhang, *Opt. Lett.*, 2021, **46**, 3448.
73 Y. Lu, P. Li, W. Xie, Y. Duan, S. Xu and J. Zhang, *Opt. Lett.*, 2021, **46**, 2597.
74 K. Zhang, D. Zhou, J. Qiu, Z. Long, R. Zhu, Q. Wang, J. Lai, H. Wu and C. Zhu, *J. Am. Ceram. Soc.*, 2020, **103**, 2463.
75 Y. Duan, P. Li, Y. Lu, X. Wang, S. Xu and J. Zhang, *Opt. Lett.*, 2021, **46**, 3580.
76 Y. Ye, W. Zhang, Z. Zhao, J. Wang, C. Liu, Z. Deng, X. Zhao and J. Han, *Adv. Opt. Mater.*, 2019, **7**, 1801663.
77 Y. Zhou, C. Liu, Z. Zhao, W. Zhang, K. Li, Y. Ye, C. F. Zhu and X. G. Meng, *J. Alloys Compd.*, 2020, **827**, 154349.
78 S. Yuan, D. Chen, X. Li, J. Zhong and X. Xu, *ACS Appl. Mater. Interfaces*, 2018, **10**, 18918.
79 Y. Liu, W. Chen, J. Zhong and D. Chen, *J. Eur. Ceram. Soc.*, 2019, **39**, 4275.
80 X. Li, C. Yang, Y. Yu, Z. Li, J. Lin, X. Guan, Z. Zheng and D. Chen, *ACS Appl. Mater. Interfaces*, 2020, **12**, 18705.
81 E. Erol, O. Kıbrıslı, M.Ç. Ersundu and A. E. Ersundu, *Chem. Eng. J.*, 2020, **401**, 126053.

82 B. Ai, C. Liu, J. Wang, J. Xie, J. Han and X. Zhao, *J. Am. Ceram. Soc.*, 2016, **99**, 2875.
83 X. Di, Z. Hu, J. Jiang, M. He, L. Zhou, W. Xiang and X. Liang, *Chem. Commun.*, 2017, **53**, 11068.
84 D. Chen, S. Yuan, X. Chen, J. Li, Q. Mao, X. Lia and J. Zhonga, *J. Mater. Chem. C*, 2018, **6**, 6832.
85 S. Chen, *J. Mater. Sci: Mater. Electron.*, 2019, **30**, 19536.
86 P. Li, W. Xie, W. Mao, Y. Tian, F. Huang, S. Xu and J. Zhang, *J. Mater. Chem. C*, 2020, **8**, 473.
87 P. Li, W. Xie, W. Mao, Y. Tian, F. Huang, S. Xu and J. Zhang, *J. Alloys Compd.*, 2020, **817**, 153338.
88 Y. Wang, R. Zhang, Y. Yue, S. Yan, L. Zhang and D. Chen, *J. Alloys Compd.*, 2020, **818**, 152872.
89 K. Weng, N. Long, Y. Guo, Q. Jiao, S. Dai, C. Lin, *et al.*, *J. Eur. Ceram. Soc.*, 2020, **40**, 4148.
90 M. P. Arciniegas, A. Castelli, S. Piazza, S. Dogan, L. Ceseracciu, R. Krahne, M. Duocastella and L. Manna, *Adv. Funct. Mater.*, 2017, **27**, 1701613.
91 C. Zou, J. Zheng, C. Chang, A. Majumdar and L. Y. Lin, *Adv. Opt. Mater.*, 2019, **7**, 1900558.
92 F. Li, W. Zhu, C. Bao, T. Yu, Y. Wang, X. Zhou and Z. Zou, *Chem. Commun.*, 2016, **52**, 5394.
93 T. Jeon, H. M. Jin, S. H. Lee, J. M. Lee, H. I. Park, M. K. Kim, K. J. Lee, B. Shin and S. O. Kim, *ACS Nano*, 2016, **10**, 7907.
94 S. J. Kim, J. Byun, T. Jeon, H. M. Jin, H. R. Hong and S. O. Kim, *ACS Appl. Mater. Interfaces*, 2018, **10**, 2490.
95 I. Konidakis, T. Maksudov, E. Serpetzoglou, G. Kakavelakis, E. Kymakis and E. Stratakis, *ACS Appl. Energy Mater.*, 2018, **1**, 5101.
96 E. Serpetzoglou, I. Konidakis, G. Kakavelakis, T. Maksudov, E. Kymakis and E. Stratakis, *ACS Appl. Mater. Interfaces*, 2017, **9**, 43910.
97 X. Huang, Q. Guo, D. Yang, X. Xiao, X. Liu, Z. Xia, F. Fan, J. Qiu and G. Dong, *Nat. Photonics*, 2020, **14**, 82.
98 X. Huang, Q. Guo, S. Kang, T. Ouyang, Q. Chen, X. Liu, Z. Xia, Z. Yang, Q. Zhang, J. Qiu and G. Dong, *ACS Nano*, 2020, **14**, 3150.
99 Y. Hu, W. Zhang, Y. Ye, Z. Zhao and C. Liu, *ACS Appl. Nano Mater.*, 2020, **3**, 850.
100 Y. Du, X. Wang, D. Shen, J. Yuan, Y. Wang, S. Yan, S. Han, Y. Tao and D. Chen, *Chem. Eng. J.*, 2020, **401**, 126132.
101 Q. Jing, Y. Xu, Y. Su, X. Xing and Z. Lu, *Nanoscale*, 2019, **11**, 1784.
102 K. Shinozaki and N. Kawano, *Sci. Rep.*, 2020, **10**, 1237.
103 N. Kawano, K. Shinozaki, D. Nakauchi, H. Kimura and T. Yanagida, *J. Appl. Phys.*, 2020, **127**, 213103.
104 I. Konidakis, K. Brintakis, A. Kostopoulou, I. Demeridou, P. Kavatzikidou and E. Stratakis, *Nanoscale*, 2020, **12**, 13697.
105 I. Konidakis, E. Skoulas, A. Papadopoulos, E. Serpetzoglou, E. Margariti and E. Stratakis, *Appl. Phys. A*, 2018, **124**, 839.
106 L. Tao, H. Long, B. Zhou, S. F. Yu, S. P. Lau, Y. Chai, K. H. Fung, Y. H. Tsang, J. Yao and D. Xu, *Nanoscale*, 2014, **6**, 9713.
107 G. Liang, L. Tao, Y. H. Tsang, L. Zeng, X. Liu, J. Li, J. Qu and Q. Wen, *J. Mater. Chem. C*, 2019, **7**, 495.
108 R. Wei, X. Tian, H. Zhang, Z. Hu, X. He, Z. Chen, Q. Chen and J. Qiu, *J. Alloys Compd.*, 2016, **684**, 224.
109 L. Tao, B. Zhou, G. Bai, Y. Wang, S. F. Yu, S. P. Lau, Y. H. Tsang, J. Yao and D. Xu, *J. Phys. Chem. C*, 2013, **117**, 23108.
110 X. Zheng, M. Fenga and H. Zhan, *J. Mater. Chem. C*, 2013, **1**, 6759.
111 A. S. Sarkar, I. Konidakis, I. Demeridou, E. Serpetzoglou, G. Kioseoglou and E. Stratakis, *Sci. Rep.*, 2020, **10**, 15697.